JAMES | Journal of Advances in Modeling Earth Systems®

RESEARCH ARTICLE
10.1029/2021MS002602

Special Section:
Advances in scaling and modeling of land-atmosphere interactions

Semi-Coupling of a Field-Scale Resolving Land-Surface Model and WRF-LES to Investigate the Influence of Land-Surface Heterogeneity on Cloud Development

Jason S. Simon[1], Andrew D. Bragg[1], Paul A. Dirmeyer[2], and Nathaniel W. Chaney[1]

[1]Duke University, Durham, NC, USA, [2]George Mason University, Fairfax, VA, USA

Key Points:

- Large-eddy simulation is used to study fine-scale heterogeneity in land-atmosphere coupling
- Spatial patterns from rainfall increase cloud production via mesoscale circulations
- Sub-grid scale heterogeneity should ideally be included in global model parameterizations

Correspondence to:
J. S. Simon,
jason.simon@duke.edu

Citation:
Simon, J. S., Bragg, A. D., Dirmeyer, P. A., & Chaney, N. W. (2021). Semi-coupling of a field-scale resolving land-surface model and WRF-LES to investigate the influence of land-surface heterogeneity on cloud development. *Journal of Advances in Modeling Earth Systems*, *13*, e2021MS002602. https://doi.org/10.1029/2021MS002602

Received 6 MAY 2021
Accepted 29 AUG 2021

Abstract Contemporary Earth system models mostly ignore the sub-grid scale (SGS) heterogeneous coupling between the land surface and atmosphere. To aid in the development of coupled land and atmosphere SGS parameterizations for global models, we present a study of different aspects of highly realistic sub-100 km scale land-surface heterogeneity. The primary experiment is a set of simulations of September 24, 2017 over the Southern Great Plains (SGP) site using the Weather Research and Forecasting (WRF) model with 100-m horizontal resolution. The overall impact of land-surface heterogeneity is evaluated by comparing cloud and turbulent kinetic energy (TKE) production in large-eddy simulations (LESs) using heterogeneous and homogeneous surface fields (namely sensible and latent heat fluxes) specified by an offline field-scale resolving land-surface model (LSM). The heterogeneous land surface leads to significantly more cloud and TKE production. We then isolate specific sources of heterogeneity by using selectively domain-wide averaged fields in the LSM. It is found that heterogeneity in the land surface created by precipitation is effectively responsible for the increases in cloud and TKE production, while rivers and soil type have a negligible impact and land cover has only a small impact. Additional experiments modify the Bowen ratio in the surface fields and the initial wind profile of the heterogeneous case to clarify the results seen. Finally two additional days at the SGP site are simulated showing a similar increase in cloud production in heterogeneous cases.

Plain Language Summary A modern Earth system model combines an atmospheric model and land-surface model, and the two interact during a simulation. Due to computational constraints, global models today use grids where very large areas (sometimes in excess of 10,000 square kilometers) are represented by a single point, making it impossible to directly represent many important features, particularly those related to the development of clouds and rain. Approximations of these processes that cannot be represented are included by simpler sub-models called parameterizations, which often base calculations on average values over the area they are modeling. To aid in the improvement of these parameterizations, a high-resolution model (where each point represents only 0.01 square kilometers) is used to simulate three summer days in Oklahoma over a total area of 10,000 square kilometers. It is seen that simulations where the land surface has moist and dry patches from previous rain events produce more clouds than simulations where the same amount of soil moisture is evenly distributed over the entire surface. We hope that this and future work will both motivate and aid efforts to add considerations for the spatial distribution of features, in addition to their average, to the parameterizations used in Earth system models.

1. Introduction

A critical challenge in characterizing land-atmosphere interactions across scales in Earth system models (ESMs) is the non-linearity that emerges as a result of spatial heterogeneities over land (Albertson et al., 2001; Bou-Zeid et al., 2004; Clark et al., 2015; Huang & Margulis, 2013; Shao et al., 2013). These complex interactions between the land-surface processes and the underlying physical environment drive the spatial complexity of surface fluxes and states (Chaney et al., 2015; Gómez-Plaza et al., 2001; Jacobs et al., 2004; Western et al., 1999). As a result, the macroscale behavior of the water and energy cycles cannot be disentangled from their fine-scale processes and interactions. The heterogeneities that emerge over land, in turn, can play a key role in many important atmospheric processes, such as setting the atmospheric boundary layer (ABL) depth, initiating convection, and spawning mesoscale circulations (Bertoldi et al., 2013; Gutowski

et al., 2020; Kang & Bryan, 2011; Kustas & Albertson, 2003; Ntelekos et al., 2008; Timmermans et al., 2008). Further, Weaver (2004b) argue that these effects are non-negligible compared to larger-scale signals over as long as monthly timescales. Although progress is being made in understanding the role of multi-scale land heterogeneity on microscale and mesoscale meteorological processes in regional and local studies (Bertoldi et al., 2013; Huang & Margulis, 2013; Kustas & Albertson, 2003; Senatore et al., 2015; Shrestha et al., 2014; Talbot et al., 2012), its role in land-atmosphere interactions in the climate system as a whole remains mostly unknown. This is primarily due to the over-simplistic coupling between existing sub-grid parameterizations in land-surface models (LSMs) and atmospheric models (e.g., tiling schemes, Bonan et al., 2002; Chaney et al., 2018; Ducharne et al., 2000; Lawrence et al., 2019; Milly et al., 2014). Existing ESMs only exchange sub-grid spatial mean fluxes of mass and energy between the land and atmosphere while disregarding higher order sub-grid spatial statistics (e.g., spatial variance). Convection and turbulence parameterizations in atmospheric circulation models are moving toward the inclusion of higher-order SGS processes (e.g., Cloud Layers Unified By Binormals (CLUBB) and Eddy Diffusivity Mass Flux (EDMF), Golaz et al., 2002; Sušelj et al., 2013), providing an opportunity for potential coupling with the SGS heterogeneity of the land surface.

There have been many modeling studies on heterogeneous land surfaces and their effects on atmospheric dynamics, primarily using idealized surface flux fields and initial atmospheres. Pielke Sr (2001) gives a very thorough theoretical background and review of the earlier work studying the effect of heterogeneous spatial distributions of sensible and latent heat fluxes from the land surface on the development of cumulus convective rainfall in the atmosphere. The general consensus from LES studies of heterogeneous land-atmosphere interactions is that surface patterns comprised of marked areas of either high sensible heat flux or high latent heat flux (typically resulting from, or an idealization of, underlying patterns of soil moisture and/or vegetation) will lead to secondary mesoscale circulations. These circulations tend to transport moist air from areas with high latent heat fluxes to areas with high sensible heat fluxes where it can be lifted through the ABL, leading to cloud production over the drier land surfaces (Avissar & Liu, 1996; Cheng & Cotton, 2004; Esau & Lyons, 2002; Garcia-Carreras et al., 2011; Hadfield et al., 1991; Han, Brdar, Raasch, & Kollet, 2019; Hohenegger et al., 2009; Huang & Margulis, 2013; Lee et al., 2019; Shen & Leclerc, 1995; van Heerwaarden & de Arellano, 2008). The clouds produced by the aforementioned circulation process tend to be deeper and more localized than those produced by homogeneous surfaces, leading to larger overall liquid water path (LWP) values but lower overall cloud cover percentages.

The necessary conditions of the land-surface heterogeneity to trigger secondary circulations are not fully established, though it is generally agreed that larger differences between the sensible heat fluxes in the warm and cool patches will produce stronger circulations. It is also generally agreed that the spatial scale of the coherent warm and cool patches must be of a sufficient size before circulations can be triggered, though with minimal consensus on more specific criteria (Albertson et al., 2001; Chen & Avissar, 1994; Hadfield et al., 1992; Han, Brdar, Raasch, & Kollet, 2019; Huang & Margulis, 2013; Kang, 2016, 2020; Kang & Ryu, 2016; Shen & Leclerc, 1995; Patton et al., 2005; Sühring et al., 2014; Timmermans et al., 2008; Trier et al., 2004). Many studies conclude simply that larger spatial scales produce stronger circulations, while others find that there is an optimal scale of land-surface heterogeneity for cloud production after which further increases have a homogenizing effect. The boundary-layer depth is commonly suggested as an optimal scale, though it is argued by van Heerwaarden et al. (2014) that this is too simplistic of a criteria.

It has been commonly reported by LES studies with idealized surface patterns that even a modest background wind will effectively eliminate the influence of land-surface heterogeneity on the atmosphere, implying that scenarios where land-surface heterogeneity would notably influence the atmosphere are, in reality, quite limited (Avissar & Schmidt, 1998; Chen & Avissar, 1994; Doran et al., 1995; Eder et al., 2015; Hadfield et al., 1992; Lee et al., 2019). However, idealized LES examples where circulations are maintained with a background wind of 7.5 m s^{-1} are shown by Raasch and Harbusch (2001), who explain that claims of wind eliminating circulations are due to experiments where the surface pattern and wind direction are such that all air parcels are continuously advected over alternating warm and cool patches. Many subsequent studies using idealized surface patterns have confirmed that the orientation of the wind direction compared to the surface heterogeneity pattern determines whether secondary circulations will be eliminated or converted to a rolling structure (Courault et al., 2007; Kang & Lenschow, 2014; Kim et al., 2002; Letzel & Raasch, 2003; Rochetin et al., 2017; Sühring et al., 2014), and multiple studies using surface patterns

based on observations have also reported that circulations are not eliminated by a synoptic wind, but instead develop perpendicular to the prevailing wind direction (Maronga & Raasch, 2013; Prabha et al., 2007; Weaver, 2004a; Weaver & Avissar, 2001). Maronga and Raasch (2013) go so far as to state that "[t]he often discussed concept of a blending height, above which the influence of the surface heterogeneity vanishes, thus cannot hold, at least under convective conditions and heterogeneity scales larger than [the boundary-layer depth]". Lynn et al. (1998), via two-dimensional deep convection simulations, found that a strong background wind increased cloud production, owing to a positive feedback between clouds rooted in the ABL and clouds rooted in the middle troposphere.

The process of heterogeneous surface fields generating mesoscale circulations which result in cloud production over drier surfaces has also been reported by many observational campaigns (Dixon et al., 2013; Garcia-Carreras et al., 2010; Lyons, 2002; Lyons et al., 1993). Taylor et al. (2011) used satellite observations to study the influence of soil moisture on the development of convective rain storms in West Africa, concluding that soil moisture variations at spatial scales ~10 – 40 km strongly control storm development in the region. Taylor et al. (2012) studied the feedback mechanisms between soil moisture and convective storms from global observations, finding that drier soils are more likely to produce afternoon rainfall events while wetter soils show no preference for rain development. They note that this result is in contrast to many weather and climate models that use convective parameterizations, which show a preference for rainfall development over wetter soils; a modeling study by Hohenegger et al. (2009) demonstrates the tendency of convective parameterizations to produce clouds over wetter soils while higher-resolution, convection-resolving models produce clouds over drier soils. Phillips and Klein (2014) studied the Southern Great Plains (SGP) site and found that, while large-scale forcings tend to dominate, there are some cases where local feedbacks from the surface play a role in the atmosphere, particularly as soil dries after a precipitation event. Koster et al. (2003) made an argument for soil moisture heterogeneity effecting precipitation by comparing observations to features in global model results which were known (in the model) to be produced by surface heterogeneity. Low-level flight observations by Dixon et al. (2013) found that circulations generated by soil moisture heterogeneity were persistent over the range of observed background winds (up to $\approx 5\ \mathrm{m\ s^{-1}}$). While the study here focuses primarily on cloud production, the impact of land-surface heterogeneity on the overall Earth system is not isolated to convection. For example, Mendes and Prevedello (2020) suggest, based on analysis of satellite observations, that secondary circulations between patches of different vegetation types has a cooling effect on surface temperatures, and Marsham et al. (2008) used aircraft observations and LES to demonstrate the significance of heterogeneity-induced mesoscale circulations on dust transport in the Sahara.

To aid in the development of an effective sub-grid coupling between the modeled land-surface and atmospheric heterogeneity in ESMs, more must be known about the coupling between land-surface heterogeneity and atmospheric dynamics. While it is generally established that heterogeneous land-surfaces can generate secondary circulations which alter cloud characteristics and production rates, many key specifics relevant to parameterizations in global models are unclear. To this end, the study presented here uses output from HydroBlocks, a field-scale resolving LSM, to drive the surface of the Weather Research and Forecasting (WRF) model, run in LES mode, over the SGP site using initial profiles and large-scale heat and moisture fluxes based on observations. The result is a study on the coupling between a realistic land surface and the ABL development over a diurnal cycle, with a specific interest in the role of different sources of land-surface heterogeneity on cloud production at scales which are SGS in a global model. A domain area of 100×100 $\mathrm{km^2}$ is used, which allows domain-wide mean values to be taken as a representation of a grid-scale value in a global model and the effects of land-surface heterogeneity, which would be SGS on a climate-scale grid, to be studied directly via LES. With this study, we aim to help to answer three key questions toward the development of global-scale parameterizations which consider SGS heterogeneity. First, are emergent mesoscale circulations between wet and dry areas observed when using realistic fields for the surface fluxes, background wind, and synoptic fluxes? If so, are the resulting effects significant on the macroscale (domain-wide) signal for a domain size comparable to a global model grid cell? Finally, what is the relative impact of the different sources of heterogeneity in the LSM (e.g., soil type, rivers and surface water, soil moisture, etc.) on the macroscale signal?

The first experiment here is a pair of simulations of September 24, 2017: the first simulation uses the high-resolution HydroBlocks land surface (described in Section 2) while the second spatially homogenizes the land surface by using domain-averaged values at each grid point (Section 3.1). Cases are then considered where only certain land-surface features are represented heterogeneously in the driving HydroBlocks simulation, generating different scales of surface heterogeneity (Section 3.2). Additional heterogeneous cases are also considered which adjust the Bowen ratio at the surface or the initial wind profile (Section 3.3). Finally, the primary heterogeneous versus homogeneous experiment is repeated for simulations of June 10, 2016 and July 16, 2017 with a brief analysis (Section 3.4).

2. Model Description

2.1. WRF

Atmospheric simulations are conducted using version 3.8.1 of the WRF model (Skamarock et al., 2008) as an LES (WRF-LES). Model settings largely follow those used in the LES ARM Symbiotic Simulation and Observation Workflow (LASSO) campaign (W. Gustafson et al., 2019; W. I. Gustafson et al., 2020), which is a publicly available data set of LES cases over the SGP site. The key difference between the LASSO simulations and those presented here is the specification of heterogeneous surface conditions. The LASSO simulations use spatially uniform, time-evolving surface fields for sensible heat flux, latent heat flux, and skin temperature (specified directly), as well as a spatially uniform and constant momentum drag coefficient. Here, heterogeneous cases use two-dimensional, time-evolving surface fields for sensible heat flux, latent heat flux, skin temperature (found via specified emissivity and upward longwave radiation fields), albedo, and momentum drag coefficient, all obtained from the HydroBlocks LSM described in Section 2.2. The sensible and latent heat fluxes, and drag coefficient are used directly by the WRF dynamics, while the skin temperature, emissivity, and albedo are used by the radiation scheme. As in the LASSO simulations, there is no feedback from the atmosphere to the land surface in the LES; the HydroBlocks LSM is run offline and the output surface fields are specified as the bottom boundary in the WRF model. Other notable differences between the WRF settings used here and those used by LASSO are the expansion of the domain to 100×100 km^2 (where the LASSO domain is 25×25 km^2), the use of the isotropic three-dimensional Smagorinsky-Lilly turbulence closure model (where LASSO uses the isotropic three-dimensional Deardorff model), the specification of two-dimensional latitude and longitude fields (where LASSO considers every grid point to be at the same latitude and longitude), and the inclusion of a Coriolis forcing (where LASSO specifies $f = 0$).

Following the LASSO configuration, simulations use the Thompson graupel microphysics scheme and the RRTMG radiation scheme (though surfaces are specified offline by HydroBlocks) with the cumulus and PBL schemes turned off. The horizontal resolution is $\Delta_{x,y} = 100$ m with a timestep of 0.5 s. The domain is approximately 14.5 km tall with 227 vertical levels and a vertical resolution of $\Delta_z = 30$ m in the lower 5 km of the column. Periodic boundary conditions are used in both lateral directions and a w-Rayleigh damping layer is applied in the upper 2 km of the column. The LES domain uses a flat bottom boundary, though terrain is considered by the offline HydroBlocks simulation for subsurface and surface routing. Initial profiles for potential temperature, water vapor mixing ratio, and lateral velocity components are obtained from the LASSO database and are applied uniformly to the domain. A relatively unique feature of the LASSO WRF simulations is the inclusion of large-scale heat and moisture flux profiles that are applied uniformly on every column in the grid at each time step as an additional contribution to the respective tendency equations, allowing the use of a single non-nested domain while still providing considerations for large-scale meteorology. Forcing data for these large-scale fluxes are also obtained from the LASSO database.

2.2. HydroBlocks

HydroBlocks is a field-scale resolving land-surface model (Chaney, Metcalfe, & Wood, 2016) that accounts for the water, energy, and carbon balance to solve land-surface processes at high spatial and temporal resolutions. HydroBlocks leverages the repeating patterns that exist over the landscape (i.e., the spatial organization) by clustering areas of assumed similar hydrologic behavior into hydrologic response units (HRUs). The simulation of these HRUs and their spatial interactions allows the modeling of the water and energy cycles at field scales (30 m) over regional to continental extents (Chaney et al., 2020; Chaney, Metcalfe, &

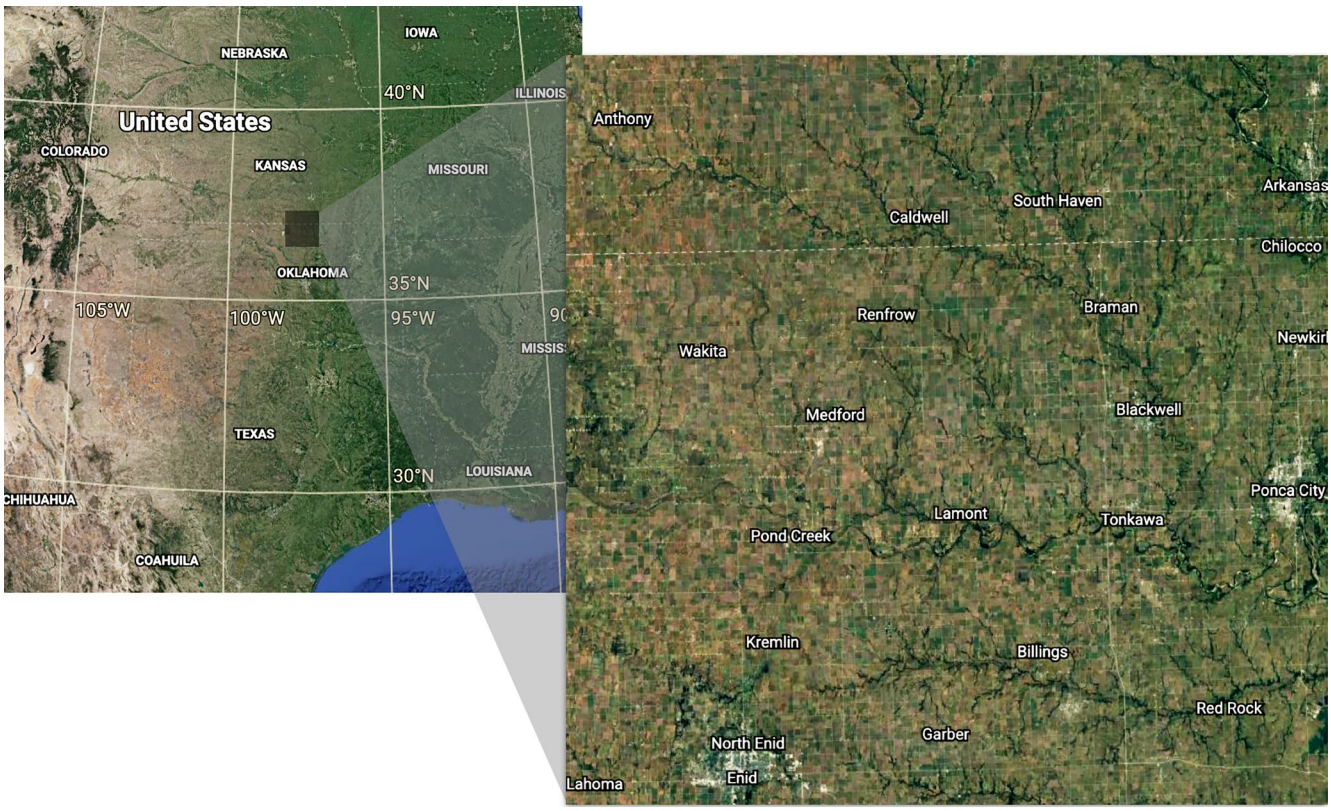

Figure 1. Map of the simulation domain, centered at the SGP site.

Wood, 2016; Vergopolan et al., 2020). The core of HydroBlocks is the Noah-MP vertical land surface scheme (Niu et al., 2011). HydroBlocks applies Noah-MP in an HRU framework to explicitly represent the spatial heterogeneity of surface processes down to field scales. At each timestep, the land-surface scheme updates the hydrologic states at each HRU; and the HRUs dynamically interact laterally via subsurface flow. Furthermore, the fine-scale river network is modeled via a reach-based kinematic wave with a two-way coupling between the HRUs and their corresponding channels.

For this study, HydroBlocks is spun up for two years and uses high-resolution (30 m) soil type and land cover maps from the Probabilistic Remapping of SSURGO (POLARIS) (Chaney et al., 2019; Chaney, Wood, et al., 2016) and National Land Cover Database (NLCD) (Homer et al., 2012) datasets, respectively, and one-eighth degree NLDAS-2 meteorology (Cosgrove et al., 2003; Mitchell et al., 2004) with NCEP Stage-IV radar rainfall (~4 km) data (Lin & Mitchell, 2005). The hourly state of the land surface produced by HydroBlocks for the period of interest is then used to specify surface values in the WRF model for: sensible heat flux, latent heat flux, momentum drag coefficient, albedo, emissivity, and upward longwave radiation. Surface skin temperature is then diagnosed from emissivity and upward longwave radiation. For the homogeneous cases, skin temperature is diagnosed from mean values of upward longwave radiation and emissivity, rather than a domain-average of skin temperature directly. For consistency, surface-flux fields are adjusted so that the domain-wide averages match the time-evolving scalar surface fluxes specified by the LASSO campaign, which are from the observationally improved VARANAL data set.

3. Results

Simulations are performed on a 100×100 km^2 domain over the SGP site, centered at 36.6 N, 97.5 W. The domain is largely cultivated cropland and grassland, with a few small urban areas and a tributary of the Arkansas River running primarily west-east through the domain (Figure 1). Comparisons between cases are made primarily by evaluating the differences in the development of LWP in time and space. LWP is of

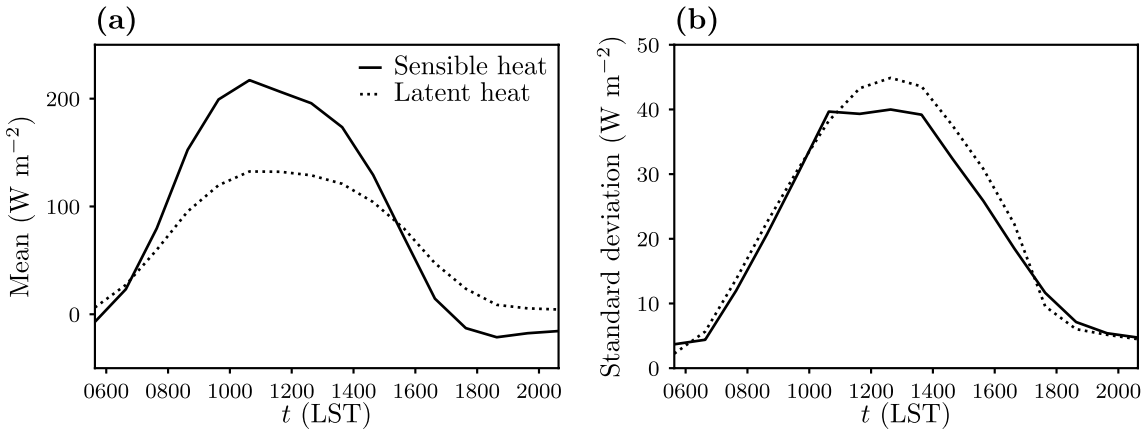

Figure 2. Time series of the surface sensible heat and latent heat fluxes used for the September 24, 2017 simulations: (a) domain mean for heterogeneous and homogeneous cases, (b) standard deviation for the heterogeneous case.

key interest because it serves as a proxy for cloud production and has a high relevance to radiation (Khanal et al., 2020; Sengupta et al., 2003). The LWP and TKE fields presented here are time-averaged values over the previous 10 min interval, sampled every 30 s. On the discretized WRF grid, our measure of LWP is found as

$$\mathrm{LWP} = \sum_z \rho_a q_l \Delta_z \quad [\mathrm{kg\,m^{-2}}] \tag{1}$$

where ρ_a is moist air density, q_l is liquid water mixing ratio, and z is the vertical direction.

The temporal development of vertically integrated, mass-coupled TKE is also compared between cases, serving as a metric for general activity in ABL development. For brevity, hereafter "TKE" may be assumed to refer to the vertically integrated, mass-coupled form unless otherwise stated. On the discretized WRF grid, our vertically integrated measure of mass-coupled TKE is found as

$$\mathrm{TKE} = \sum_z \rho_a \left[\frac{1}{2}\left(u'^2 + v'^2 + w'^2\right)\right]\Delta_z \quad [\mathrm{kg\,s^{-2}}] \tag{2}$$

where u, v, and w are the velocity components in the x (west-east), y (south-north), and z directions, respectively, and a primed variable indicates deviation from the mean value in the (x, y) plane.

3.1. Heterogeneous Versus Homogeneous

The primary day considered is September 24, 2017. This day was chosen due to the appreciable spatial heterogeneity in the LSM simulations. Following the LASSO setup, simulations are run for 15 h beginning at 0538 Local Solar Time (LST) (1200 UTC). Over the 100×100 km^2 domain, for both the heterogeneous and homogeneous simulations, the average sensible heat flux peaks at $t \approx 1100$ LST with a magnitude of approximately 215 W m^{-2}, and the domain-averaged latent heat flux peaks at the same time with a magnitude of approximately 130 W m^{-2} (Figure 2a). In the heterogeneous case the standard deviations of the sensible and latent heat fluxes both peak at $t \approx 1300$ LST with values of approximately 40 and 45 W m^{-2}, respectively (Figure 2b). Both simulations are initialized with the same domain-wide profiles for potential temperature, water vapor mixing ratio, and lateral velocity components, shown in Figure 3. The initial profile is stable with a water vapor mixing ratio of $\mathcal{O}(10$ g kg$^{-1})$ in the lower 4 km and a wind profile which is predominantly south-north with $v \approx 15$ m s^{-1} in the lower 10 km of the column. The bulk lateral flow is maintained by the periodic boundary conditions, allowing the profile to develop unconstrained. The large-scale heat and moisture fluxes are predominantly positive influxes over the duration of the simulation, with peak values $\approx 6 \times 10^{-5}$ K s^{-1} and $\approx 4 \times 10^{-5}$ g kg^{-1} s^{-1}, respectively (not shown).

Maps of the surface sensible heat flux and latent heat flux used to drive the WRF-LES surface, upscaled to $\Delta_{x,y} = 100$ m from the HydroBlocks output, are shown in Figure 4 at $t = 1238$ LST, corresponding to the peak standard deviations for sensible and latent heat fluxes in the diurnal cycle. This day was chosen for the

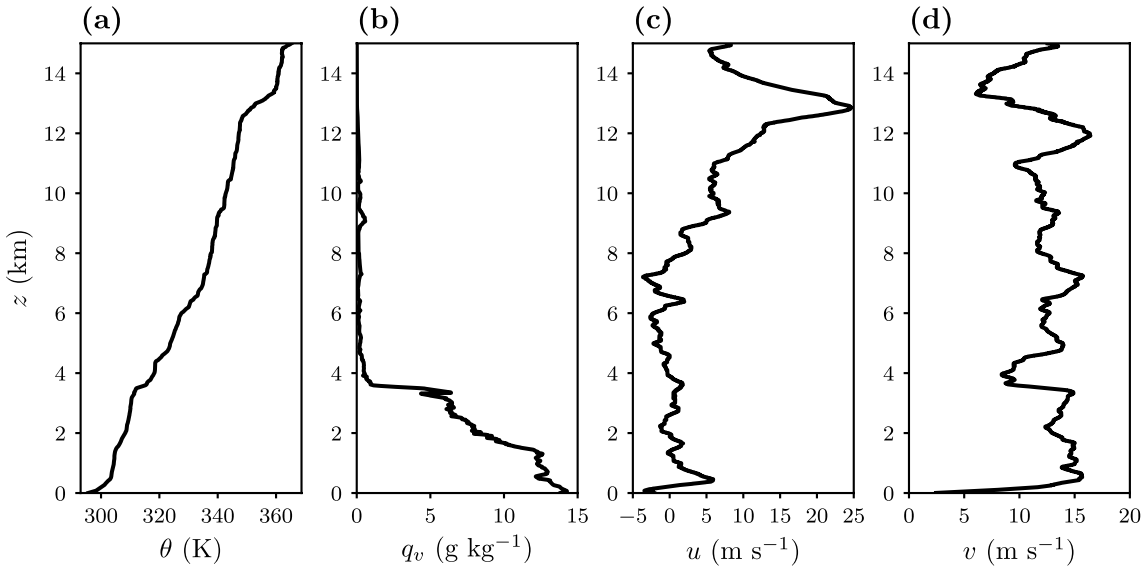

Figure 3. Initial profiles used for the September 24, 2017 simulations: (a) potential temperature, (b) water vapor mixing ratio, (c) u-velocity, and (d) v-velocity.

large moist patch in the east of the domain, which is a result of a rain event that occurred a few days before. Surface fields in the LES are specified from HydroBlocks every hour (UTC) on the hour and are linearly interpolated in time at each timestep in between. The homogeneous case specifies the domain-averaged value of the aforementioned surface fields at each grid point, calculated at each timestep. It is worth noting that while the spatial patterns of rivers and subsurface flow are removed in the homogeneous case, their contribution to the domain-wide latent heat flux is still included (Barlage et al., 2021, present a study on the importance of resolving river and stream networks).

The heterogeneous and homogeneous simulations show a notable difference in both domain-wide LWP (Figure 5a) and vertically integrated, mass-coupled TKE (Figure 5b) in time. Both cases begin to produce liquid water in the atmosphere at $t \approx 1000$ LST, but the two cases diverge at $t \approx 1200$ LST. The heterogeneous case continues to produce liquid water more rapidly, reaching a peak over 300 g m^{-2} just after $t = 1400$ LST, while the homogeneous case has a lower rate of production, reaching a peak of less than 130 g m^{-2} near 1500 LST. Production of TKE between the two cases shows similar differences, where the two

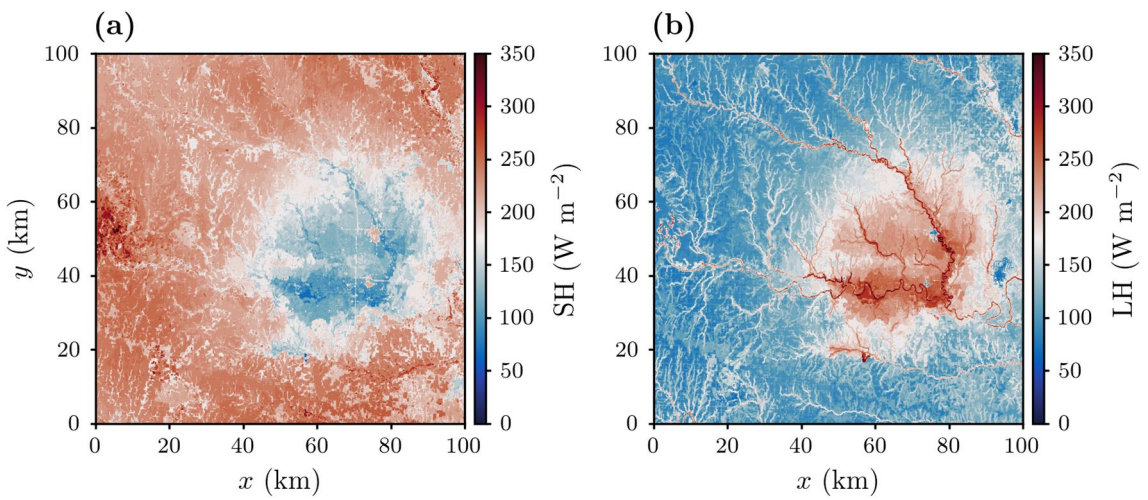

Figure 4. Heterogeneous surface values for the September 24, 2017 simulations at $t = 1238$ LST, upscaled from HydroBlocks: (a) sensible heat flux, (b) latent heat flux.

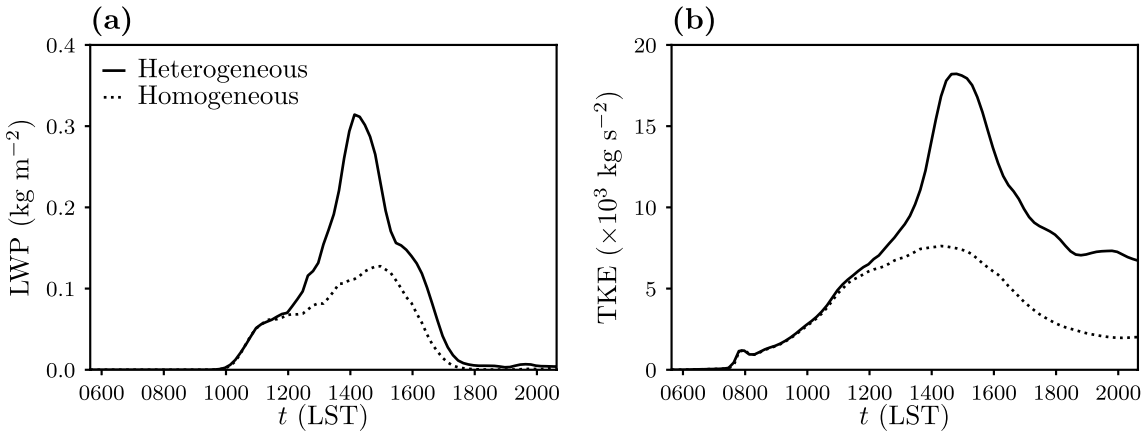

Figure 5. Domain-wide mean fields in time from the heterogeneous and homogeneous September 24, 2017 simulations: (a) Liquid water path, (b) vertically integrated, mass-coupled turbulent kinetic energy.

cases diverge again at $t \approx 1100$ LST with the heterogeneous case reaching a much larger peak value than the homogeneous case.

To examine differences in spatial liquid water production, a map of each grid point's maximum LWP value throughout the duration of the simulation is shown for the heterogeneous (Figure 6a) and homogeneous (Figure 6b) cases. The heterogeneous case shows a very strong pattern of high liquid water production in the western 30 km of the domain and low liquid water production in the eastern 70 km of the domain, while the homogeneous case is very evenly distributed throughout the domain. Recalling that this case has a large moist patch in the east of the domain, cloud production for this case demonstrates a preference for areas with a high sensible heat flux at the surface. This is similar to many previous studies where increased cloud production is achieved by emergent circulation patterns which transport moisture from areas of high latent heat flux to areas of high sensible heat flux where it is then lifted (e.g., Avissar & Liu, 1996; Hadfield et al., 1991; Han, Brdar, & Kollet, 2019; Hohenegger et al., 2009; Huang & Margulis, 2013; Lee et al., 2019; Rieck et al., 2014; Shen & Leclerc, 1995; van Heerwaarden & de Arellano, 2008). We will see in Section 3.3 that the larger local sensible heat fluxes present in the heterogeneous case alone are not sufficient to generate the levels of cloud production seen.

Emergent mesoscale circulations in the heterogeneous case are examined first with cross-section profiles of $u(x)$ at $t = 1408$ LST, approximately corresponding to the time of peak LWP in the domain, at $y = 50$ km (Figure 7a) and averaged over the full domain in the y direction (Figure 7b). The profiles reveal the antici-

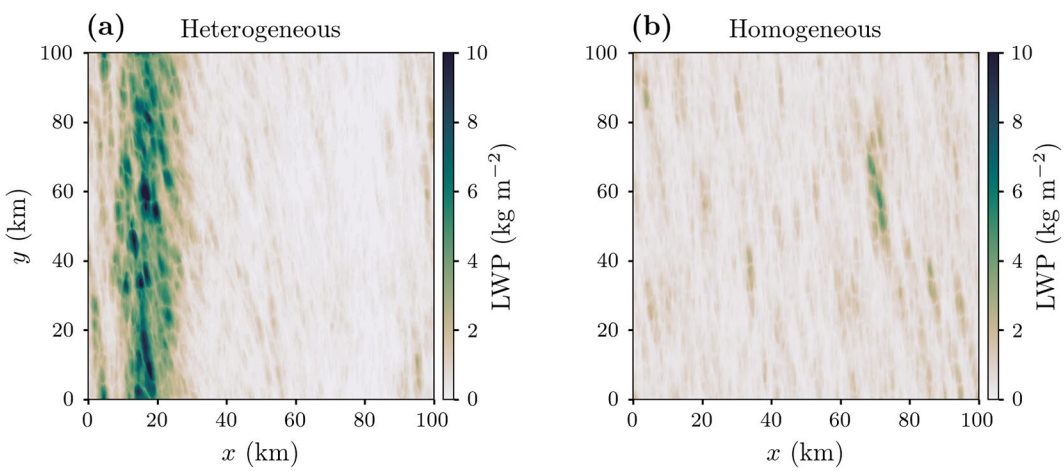

Figure 6. Maximum values of liquid water path at each grid point throughout the duration of the September 24, 2017 simulations using: (a) heterogeneous land surfaces, (b) homogeneous land surfaces.

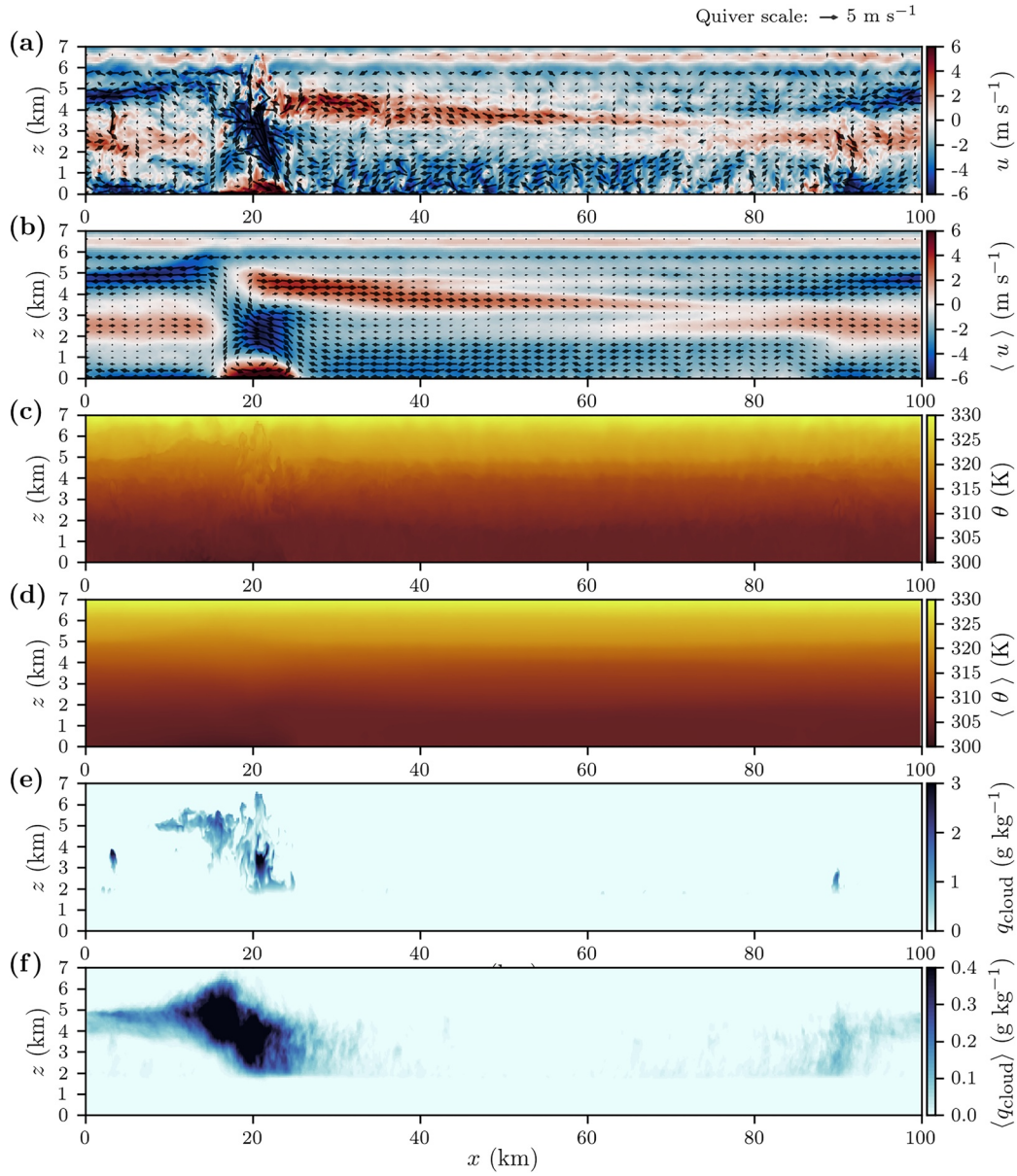

Figure 7. Profiles from the September 24, 2017 simulation using heterogeneous surfaces at $t = 1408$ LST of: (a) u-velocity along x at $y = 50$ km, (b) u-velocity along x and domain-averaged in y, (c) potential temperature along x at $y = 50$ km, (d) potential temperature along x and domain-averaged in y, (d) cloud mixing ratio along x at $y = 50$ km, (f) cloud mixing ratio along x and domain-averaged in y.

pated general circulation behavior, where flow is primarily westward in the lower 2 km of the domain with a coherent band of eastward flow aloft which reaches a height of $z \approx 5$ km at $x \approx 25$ km, gradually descending to $z \approx 3$ km over the eastern edge of the domain. The rolling structure induced by the synoptic wind (which is predominantly in the $+v$ direction) is seen very clearly in the y-averaged cross-section, centered at $x \approx 20$ km and $z \approx 1$ km. Similar cross-section profiles across x of potential temperature and cloud mixing ratio are shown for the heterogeneous case in Figures 7c–7f. Cloud production in the heterogeneous case is focused in the west of the domain reaching an average cloud top just below $z = 7$ km, with some sparser and lower clouds in the east of the domain.

Half-hourly cross-sections of u-velocity and cloud mixing ratio are shown for the heterogeneous case along $y = 50$ km from 1138 to 1538 LST in Figure 8. At 1138 LST, which is just before the LWP time series be-

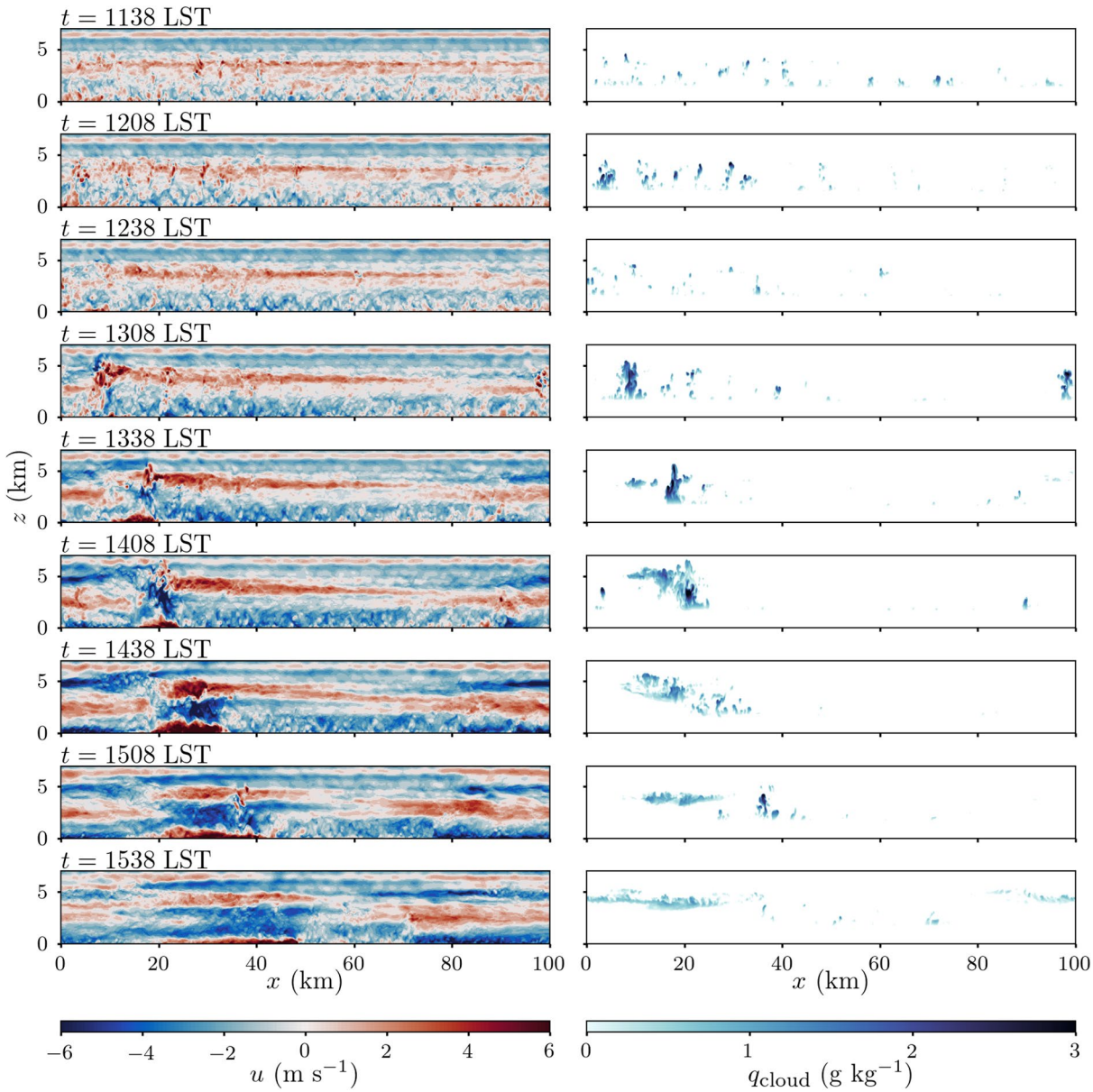

Figure 8. Profiles taken every 30 min from $t = 1038$ to 1538 LST along x at $y = 50$ km from the September 24, 2017 simulation using heterogeneous surfaces of: (left column) of u-velocity and (right column) cloud mixing ratio.

tween the two cases diverge, the profile appears relatively homogeneous, with a band of eastward flow aloft throughout the full domain width. By 1238 LST the circulation pattern is clearly visible in the flow, and by 1308 LST it is fully formed with the accompanying cloud production in the west of the domain. At 1438 LST the circulation appears to be in the early stages of decline, and the clouds aloft are spreading laterally and dissipating, and by 1538 LST both the circulation and cloud layer appear fully in their dissipation phase.

Cross-sections along x of u-velocity, potential temperature, and cloud mixing ratio are shown for the homogeneous case in (Figure 9), also at $t = 1408$ LST. The $y = 50$ km cross-section of $u(x)$ for the homogeneous case (Figure 9a) shows many clear upwelling events, but they are distributed across the full width of the domain without developing any coherent circulation pattern, as is expected of an atmosphere with a uniform surface heating. The cloud mixing ratio similarly shows a very uniform cloud pattern, producing very sparse clouds compared to the heterogeneous simulation with a much lower cloud top, below $z = 5$ km.

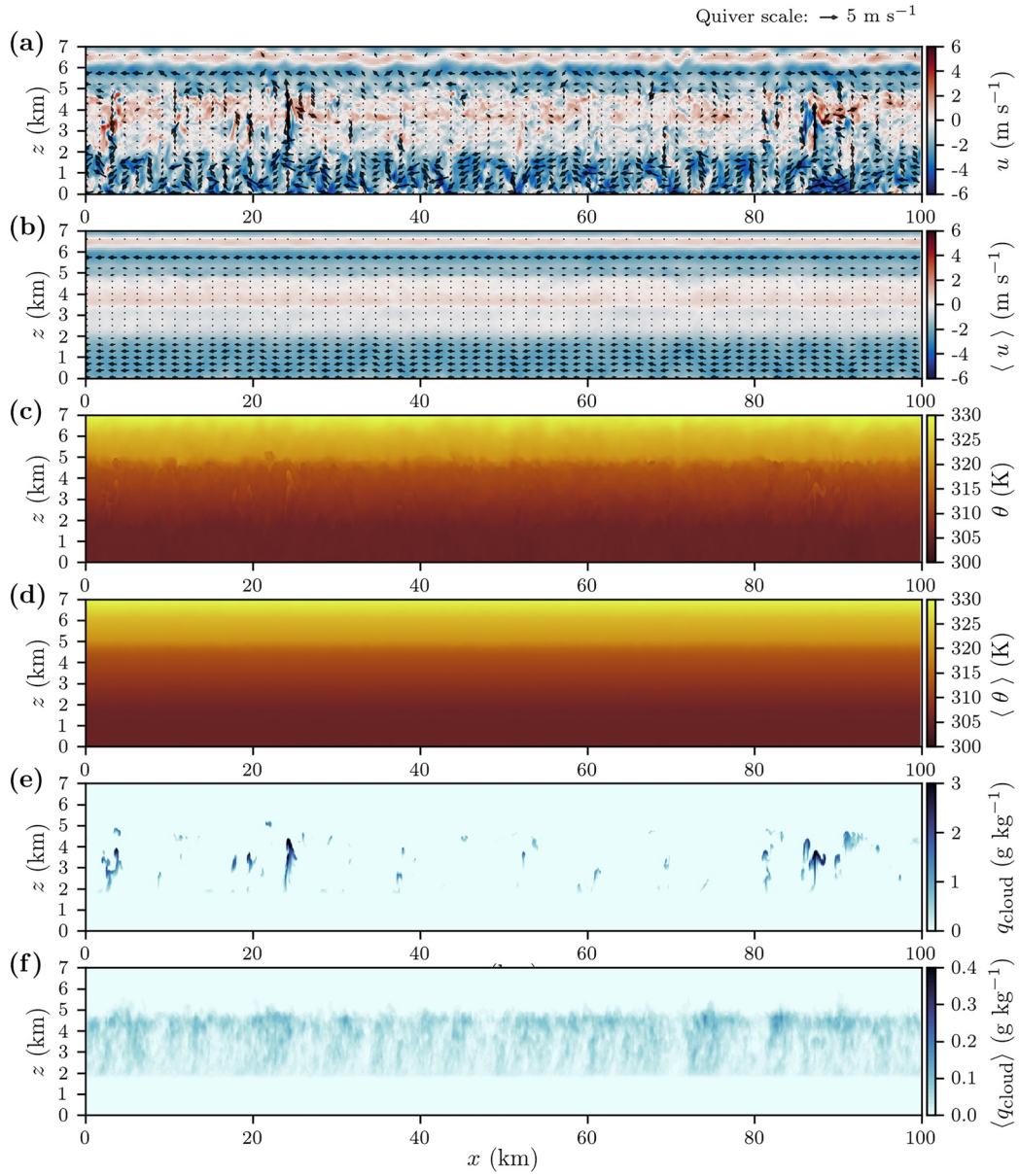

Figure 9. Profiles from the September 24, 2017 simulation using homogeneous surfaces at $t = 1408$ LST of: (a) u-velocity along x at $y = 50$ km, (b) u-velocity along x and domain-averaged in y, (c) potential temperature along x at $y = 50$ km, (d) potential temperature along x and domain-averaged in y, (d) cloud mixing ratio along x at $y = 50$ km, (f) cloud mixing ratio along x and domain-averaged in y.

Compared to the homogeneous case, liquid water production in the heterogeneous case appears to benefit from both the moist and dry patches in its surface forcing, despite them not being co-located, via the latent heat flux from the moist patch being transported laterally to drier areas with a higher sensible heat flux which then lifts the moist air past the lifted condensation level resulting in local cloud production. The homogeneous case, which has the same domain-wide total surface latent and sensible heat fluxes, is unable to generate the same cloud production without local areas of higher sensible heat flux to produce similar local updrafts for the moisture that is present in the boundary layer. The following two sections will further investigate the mechanisms driving the behavior of the heterogeneous case seen here.

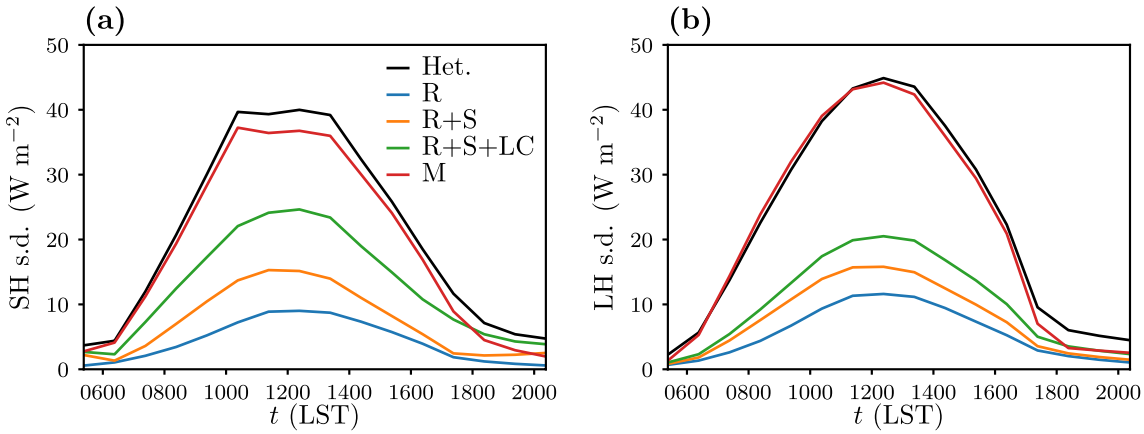

Figure 10. Time series of standard deviations of the surface fluxes used for the September 24, 2017 simulations where the land model includes heterogeneity from only rivers (R), rivers and soil type (R + S), rivers, soil type and land cover (R + S + LC), and only forcing meteorology (M): (a) sensible heat, (b) latent heat. The fully heterogeneous case is also shown for comparison.

3.2. Land-Surface Components

The heterogeneity in the surface fields used in Section 3.1 is the result of four primary sources in the HydroBlocks model: river routing and subsurface flow, soil type, land cover, and forcing meteorology. To better understand the role of land-surface heterogeneity in atmospheric dynamics we present four additional WRF simulations which use surface maps from HydroBlocks when considering only certain sources of heterogeneity. The first simulation (the "R" case) contains surface heterogeneity generated only by rivers and subsurface flow, using surface fields from a HydroBlocks simulation which calculates river routing and subsurface flow as normal but uses homogenized fields for soil type, land cover, and forcing meteorology. The second simulation ("R + S") follows the same methodology but the driving HydroBlocks simulation also uses the heterogeneous soil-type map. The third simulation ("R + S + LC") uses the heterogeneous land cover field in addition to rivers/subsurface flow and soil type. The fourth simulation ("M") isolates surface heterogeneity generated by the meteorology driving the LSM by homogenizing the other fields. Each case is energetically constrained so that the domain-averaged surface sensible and latent heat fluxes remain unchanged from the base cases, thus only the standard deviations and spatial scales of heterogeneity differ between these four cases and those in Section 3.1. The fully heterogeneous case from Section 3.1 is equivalent to an "R + S + LC + M" case and is used here, along with its corresponding fully homogeneous case, as a reference for comparison.

Standard deviations of surface sensible heat flux and latent heat flux in time are shown in Figures 10a and 10b, respectively. The sensible heat flux standard deviations are, very approximately, evenly spaced between 10 W m^{-2} and 40 W m^{-2} with the R case peaking at the lowest value (approximately 10 W m^{-2}), followed by the R + S and R + S + LC cases. The M case has a peak standard deviation just below the fully heterogeneous case's peak value (approximately 40 W m^{-2}). The latent heat flux standard deviations, on the other hand, have two clear groups: the R, R + S, and R + S + LC cases which have peak values from approximately 10 to 20 W m^{-2}, and the fully heterogeneous and M cases which are nearly overlapping with a peak value of approximately 45 W m^{-2}.

Maps of surface sensible heat flux and latent heat flux at t = 1238 LST for the four cases are shown in Figure 11. The R case has a largely homogeneous sensible heat flux field (Figure 11a1) and a river network visible in the latent heat flux field (Figure 11b1) which, despite appearing very heterogeneous, contains only small spatial scales of heterogeneity and spans the entire domain. The R + S case has a small visual increase in sensible and latent heat flux heterogeneity compared to the R case (Figures 11a2 and 11b2, respectively). The R + S + LC case adds considerable visual detail to the sensible heat flux (Figure 11a3) and latent heat flux (Figure 11b3) fields compared to the R + S case. The M case is largely homogeneous in both fields (Figures 11a4 and 11b4) aside from the ~ 50 km moist patch in the east of the domain, confirming that

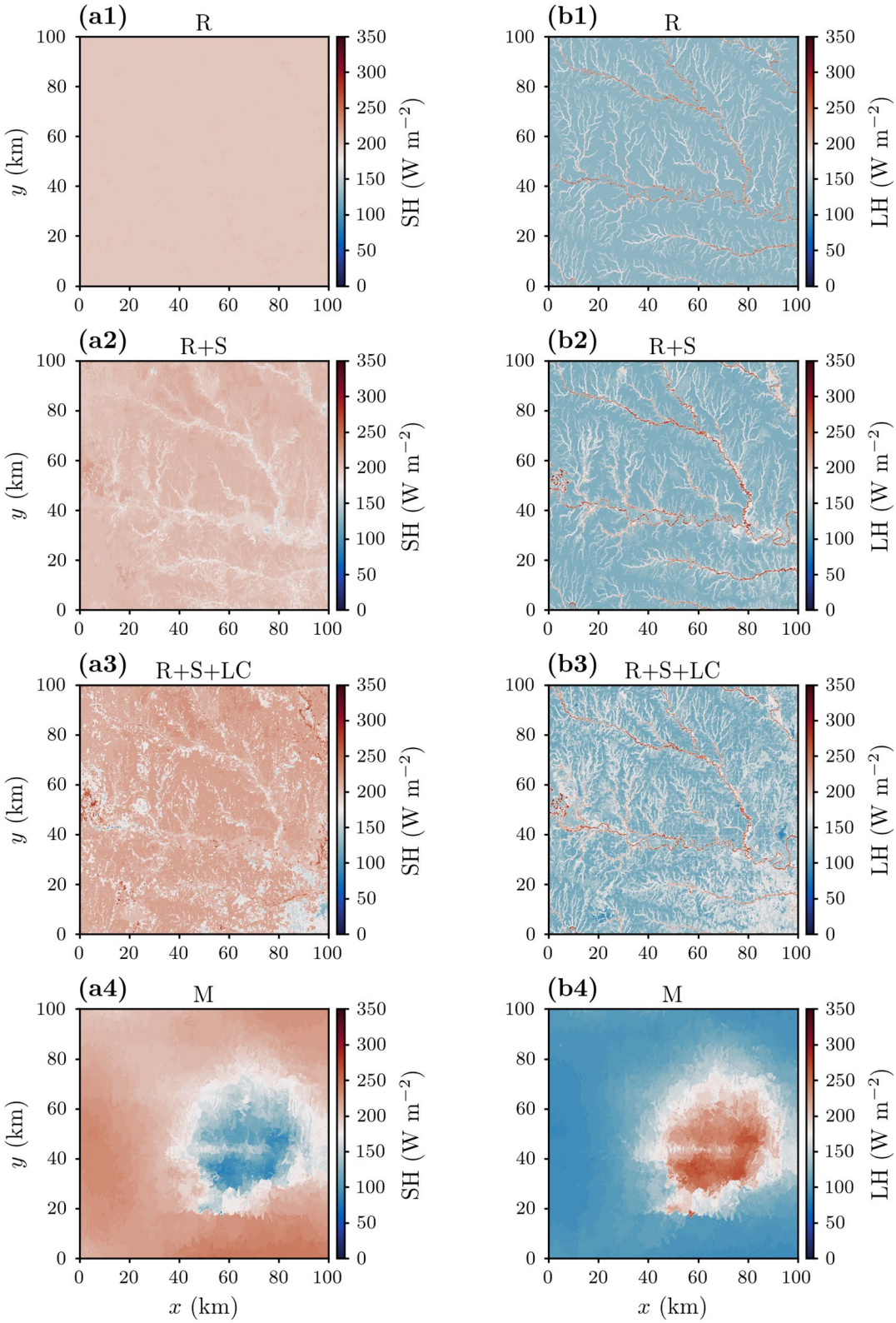

Figure 11. (column a) Surface sensible heat flux and (column b) latent heat flux fields for September 24, 2017 simulations at t = 1238 LST with land surfaces which include heterogeneity from: (row 1) only rivers (R), (row 2) rivers and soil type (R + S), (row 3) rivers, soil type and land cover (R + S + LC), and (row 4) only forcing meteorology (M).

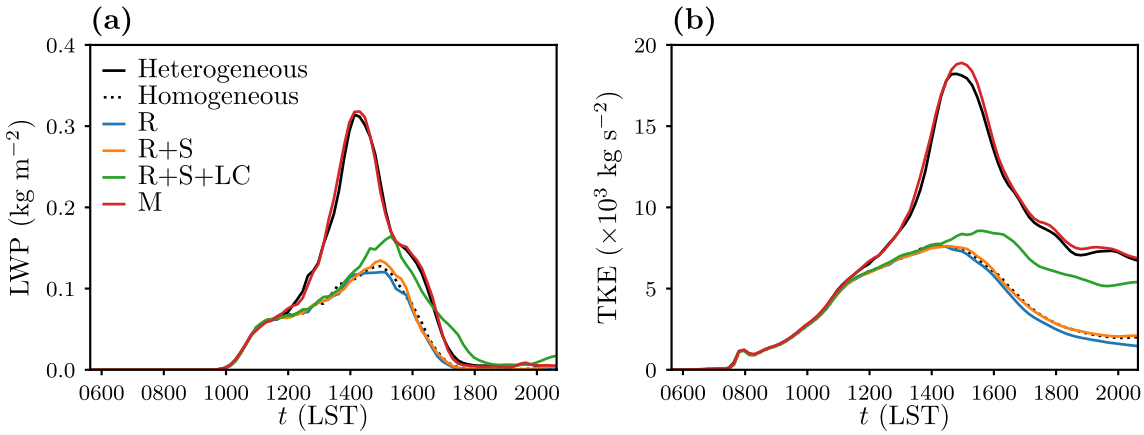

Figure 12. Domain-wide mean fields in time from the September 24, 2017 simulations where the land model includes heterogeneity from only rivers (R), rivers and soil type (R + S), rivers, soil type and land cover (R + S + LC), and only forcing meteorology (M): (a) Liquid water path, (b) vertically integrated, mass-coupled turbulent kinetic energy. The fully heterogeneous and fully homogeneous cases are also shown for comparison.

heterogeneous forcing meteorology is responsible for the larger scales of land-surface heterogeneity seen in the fully heterogeneous case.

Considering the resulting time series of LWP and TKE for these cases (Figures 12a and 12b, respectively), the R and R + S cases are nearly indistinguishable from the fully homogeneous case while the R + S + LC case follows the fully homogeneous case until $t \approx 1400$ LST but then has a larger peak than the homogeneous case for both LWP and TKE. The liquid water and TKE production are nearly identical between the M and the fully heterogeneous case with very slightly larger values in the M case, indicating that the R, S, and LC sources have a (very small) homogenizing effect on the atmospheric response to the M fields despite the fully heterogeneous case having a slightly larger standard deviation (a similar effect was reported by Zhang et al., 2010). The M case produces nearly all of its liquid water in the westernmost 40 km of the domain while the other three cases are relatively homogeneous (not shown).

It is clear in this case that heterogeneous meteorology in the LSM is the primary driver of atmospherically relevant heterogeneity in the land surface. It is also seen that the standard deviation of surface properties alone is insufficient to describe its impact on atmospheric dynamics, as demonstrated by the close agreement in LWP and TKE production between the fully homogeneous, R, and R + S cases despite significant differences in standard deviations.

3.3. Modified Bowen Ratio and Wind Profile Cases

It is shown in Section 3.1 that a circulation pattern forms between the cool/moist and warm/dry areas of the land surface in the heterogeneous case, however it is not clear how necessary the moisture transported toward the warm surface by this circulation is for the observed cloud production. Patches of high surface sensible heat fluxes relative to their surroundings have been seen in observational and modeling studies to increase local cloud production without the formation of secondary circulations (e.g., Bosman et al., 2019, and references therein). While this effect is often in the context of heterogeneity created by deforestation, it is possible that the local areas of high sensible heat flux in the heterogeneous surfaces here combined with the moisture that already exists over those areas (from the initial profile and large-scale forcing) are sufficient to generate the increased cloud production of the heterogeneous case without the formation of any secondary circulations. Such a process would also be lost in the homogeneous case, where the sensible heat flux at every grid point is set to the domain-wide mean. To evaluate these two possible explanations, we consider heterogeneous cases with all of the surface latent heat flux at each grid point converted to additional sensible heat flux at the same grid point (the "0% latent heat" case) and 80% of the surface latent heat flux at each grid point converted to additional sensible heat flux at the same grid point (the "20% latent heat" case). The conversion of latent heat to sensible heat inherently reduces the standard deviation of both the sensible and latent heat flux fields, but without reducing local maxima of surface sensible heat flux. These

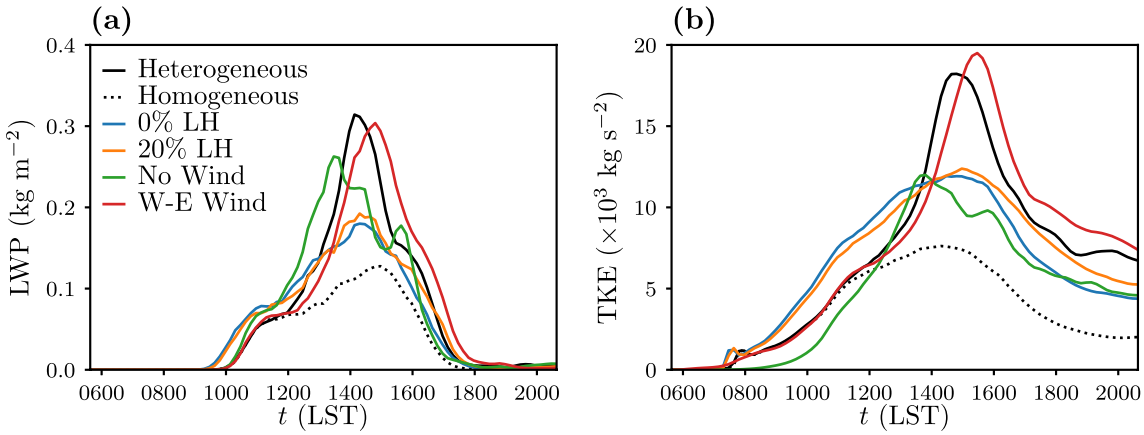

Figure 13. Domain-wide mean fields in time from the 0% LH, 20% LH, no wind, and w-e wind simulations of September 24, 2017: (a) Liquid water path, (b) vertically integrated, mass-coupled turbulent kinetic energy. The fully heterogeneous and fully homogeneous cases are also shown for comparison.

two cases, compared to the base heterogeneous case, are used to isolate the effect of larger local sensible heat fluxes on moisture from sources other than surface latent heat fluxes (i.e., from the initial profile and large-scale forcing).

Additionally, simulations in previous sections have all used the same initial wind profile which has a south-north component $v \approx 15\,\mathrm{m\,s^{-1}}$ throughout the column. To evaluate the effect of the wind profile, we consider a case with no wind in the initial profile (the "no wind" case) and a case where the wind at each vertical level of the initial profile is re-oriented to be purely west-to-east (the "w-e wind" case). Both modified-wind cases use the unmodified heterogeneous land surface fields. The motivation for these cases is to add context to the results in Section 3.1 compared to previous studies available in the literature.

Time series of LWP and TKE for all four cases are shown in Figures 13a and 13b, respectively. The increase in surface sensible heat flux in the 0% and 20% latent heat cases slightly speeds up the onset of liquid water production and significantly increases the TKE production in the first six hours compared to the fully heterogeneous and homogeneous cases. The 0% and 20% latent heat cases produce more liquid water and TKE throughout the simulation than the fully homogeneous case, but are surpassed by the fully heterogeneous case after $t \approx 1300$ LST. The 20% latent heat case produces slightly more liquid water and TKE than the 0% latent heat case throughout the simulation. The 0% latent heat case produces clouds throughout the domain but with the thickest clouds in the east (Figure 14a), while the and 20% latent heat cases retains the heterogeneous case's general preference for cloud production in the west of the domain (Figure 14b). It is noteworthy that the 0% and 20% latent heat cases both ultimately produce much less TKE than the heterogeneous case despite significant increases to surface sensible heat flux. It is also interesting that in the 0% latent heat case any liquid water produced is solely from moisture that exists in the initial profile or that is introduced by the large-scale moisture flux forcing, both of which are applied uniformly in the domain. Still, the 0% latent heat case is able to produce more liquid water than the fully homogeneous case or any case considered in Section 3.2.

The no wind case produces more liquid water and TKE than the homogeneous case but less than the heterogeneous case, reaching peak values earlier than both base cases. The w-e wind case shows very similar productions of liquid water and TKE to the base heterogeneous case. Maps of maximum LWP at each grid point throughout the simulation for the two modified wind cases are particularly informative. The no wind case (Figure 14c) produces very concentrated individual clouds of a spatial scale $\mathcal{O}$(1 km) which themselves are very densely distributed in space (when considering the entire 15 hours together) over the entire dry portion of the domain, including the relatively small urban areas in the middle of the moist patch. The w-e wind case (Figure 14d) shows a strong preference for liquid water production in the southern 20 km of the domain, closely resembling the base heterogeneous case's aversion to cloud production over the moist patch but realigned to the w-e wind direction.

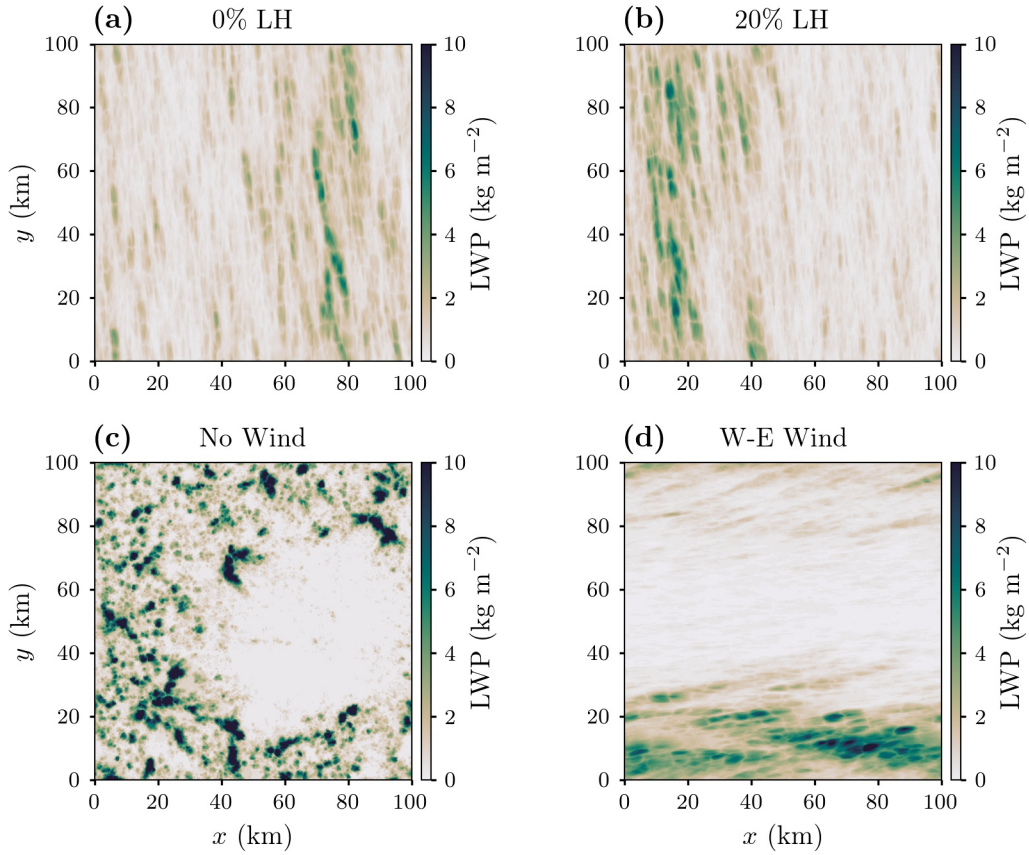

Figure 14. Maximum values of liquid water path at each grid point throughout the duration of modified September 24, 2017 simulations: (a) 0% latent heat case, (b) 20% latent heat case, (c) no wind case, (d) w-e wind case.

The result that clouds show a preferential production over warm/dry areas in the presence of land-surface heterogeneity is widely reported (e.g., Avissar & Liu, 1996; Esau & Lyons, 2002; Hohenegger et al., 2009; Huang & Margulis, 2013; Kang, 2016; Lee et al., 2019; Taylor et al., 2012; van Heerwaarden & de Arellano, 2008). The persistence of the circulation with a background wind of the magnitude used here is relatively novel, but the general result that circulations orient themselves perpendicular to the background wind direction has been both demonstrated and explained in previous studies (e.g., Prabha et al., 2007; Raasch & Harbusch, 2001; Rochetin et al., 2017; Shen & Leclerc, 1995; Sühring et al., 2014; Weaver, 2004a), though with less of a consensus. Rieck et al. (2014) state on this topic, in review, that while the role of wind is "controversial," "it is expected that too strong background winds mask the effects of land surface heterogeneities." In reality the role of wind is likely even more nuanced than can be effectively evaluated by modern LES studies, for example, a nested mesoscale-modeling study by Findell and Eltahir (2003) found that the influence of the background wind on surface fluxes, as it relates to triggering convection, can either suppress or enhance convection depending on whether it was backing or veering.

3.4. Additional Days

To justify the generality of the results seen here for September 24, 2017, two additional days at the SGP site are presented briefly for basic heterogeneous and homogeneous cases. All model settings for these cases are the same as before except for different surface fields, initial soundings, and large-scale forcings. Analysis for these cases is limited to time series of LWP.

Time series of domain-averaged surface sensible heat and latent heat fluxes for the two days are shown in Figure 15, and maps of the surface sensible and latent heat fluxes at $t \approx 1230$ LST for the two days are shown in Figure 16. Both days have land surfaces which are dominated by rainfall from previous days, but

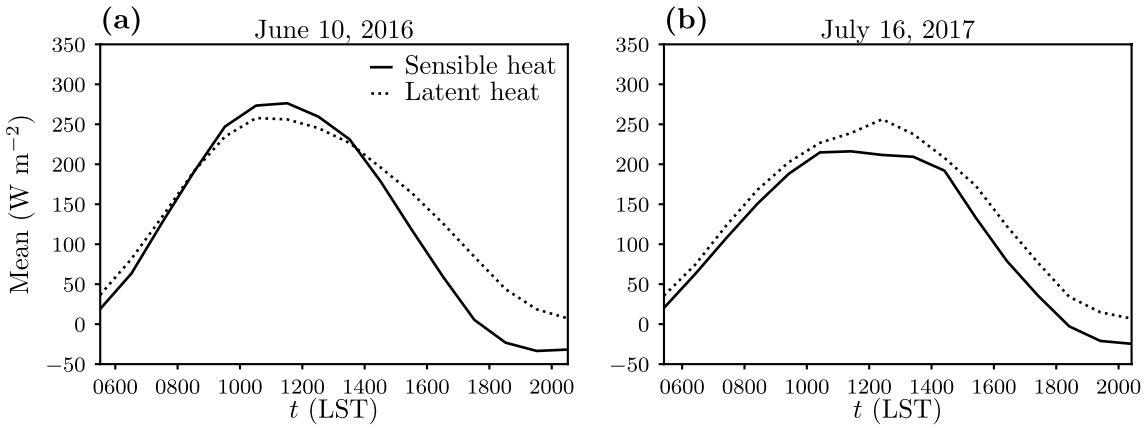

Figure 15. Time series of the domain mean surface sensible heat and latent heat fluxes used for simulations of: (a) June 10, 2016 and (b) July 16, 2017.

in different patterns from each other and from September 24, 2017. The June 10, 2016 case has a surface pattern where moist patches are present in the north-east and south-west corners of the domain (Figures 16a1 and 16b1), while the moist patch in the July 16, 2017 case dominates the eastern half of the domain (Figures 16a2 and 16b2). The initial wind profile for the June 10, 2016 case is similar in magnitude to the September 24, 2017 case (≈15 m s^{-1}), while the July 16, 2017 case has only a nominal background wind (≈1 m s^{-1}) (not shown).

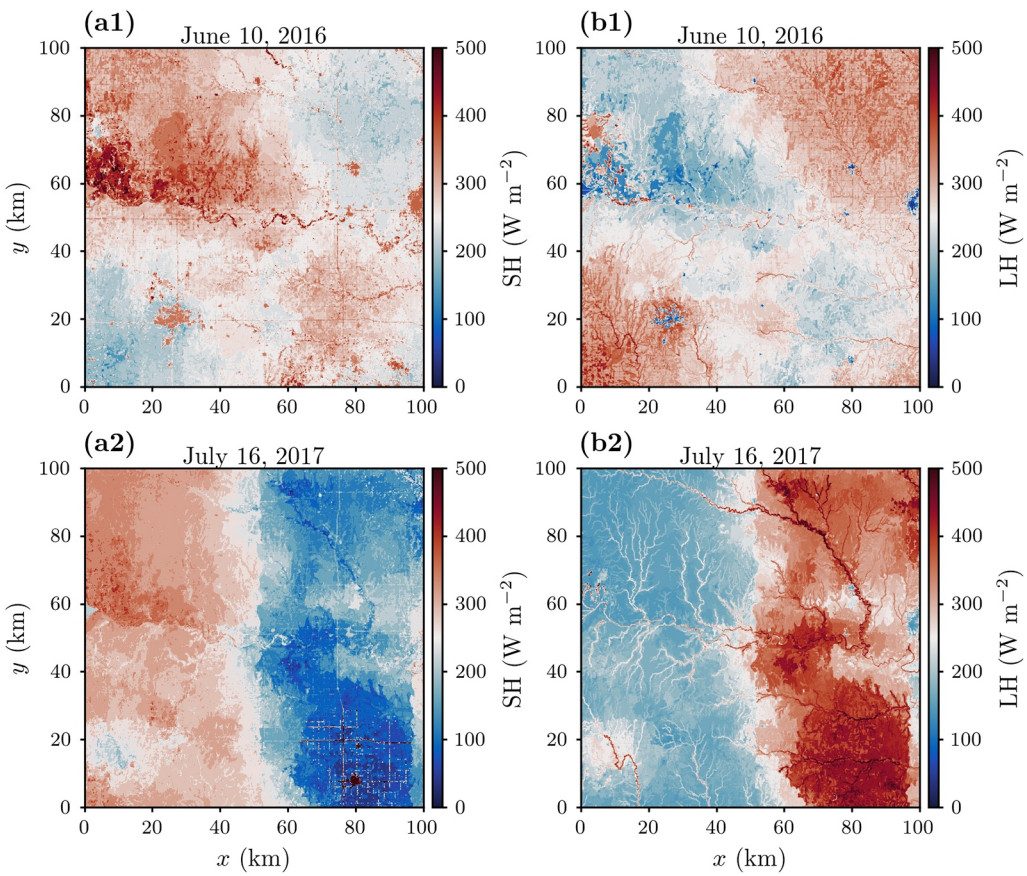

Figure 16. (column a) Surface sensible heat flux and (column b) latent heat flux fields at $t \approx 1230$ LST for simulations of: (row 1) June 10, 2016 and (row 2) July 16, 2017.

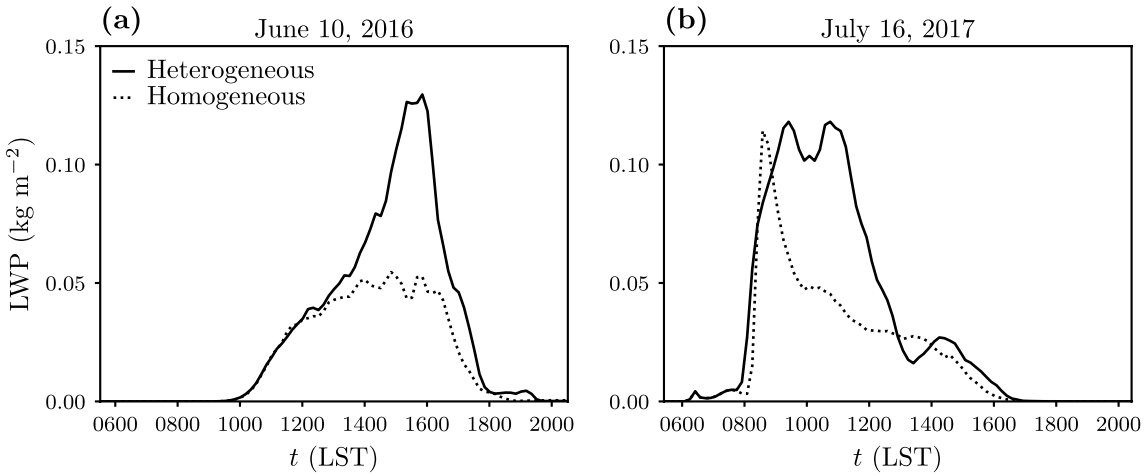

Figure 17. Domain-wide liquid water path in time from the heterogeneous and homogeneous simulations of: (a) June 10, 2016 and (b) July 16, 2017.

The time series of domain-wide LWP for heterogeneous and homogeneous simulations of both days (Figure 17) show similar behavior to the September 24, 2017 simulations, where the heterogeneous cases produce significantly more overall liquid water than their homogeneous counterparts. For all three days, initial liquid water production is very similar between heterogeneous and homogeneous cases, as is the timing of the ultimate dissipation of liquid water, but large differences are seen midday. The June 10, 2016 case is very similar to the September 24, 2017 case, where the heterogeneous and homogeneous cases begin liquid water production at $t \approx 1000$ LST with very similar rates and then diverge at $t \approx 1300$ LST when the heterogeneous case accelerates its production and ultimately reaches a much larger peak LWP value than the homogeneous case. The July 16, 2017 case shows a much different behavior, where both the heterogeneous and homogeneous cases show a huge burst of liquid water production at $t \approx 0800$ LST, with both cases reaching a very similar peak LWP value for the day before 1000 LST. The difference between the two cases for July 16, 2017 is that the homogeneous case shows a rapid decline following the initial burst of liquid water, while the heterogeneous case is able to maintain its liquid water for another four hours.

The two additional dates were selected relatively arbitrarily from the LASSO database, which has 95 days from 2015 to 2019 that are pre-selected for shallow convection, based on a spatially and temporally coarse knowledge of standard deviation in the surface heat fluxes which produced a few dozen candidate dates. That is, they were not chosen with any prior knowledge of how their heterogeneous and homogeneous cases compared. That both of these cases show a similar response in the domain-wide LWP signal to land-surface heterogeneity created by prior rain events, despite ultimately showing very different spatial patterns in the land surface over the same domain, gives a strong indication of the importance of spatial patterns of heterogeneity in land-atmosphere coupling as it specifically relates to SGS parameterizations for global ESMs.

4. Discussion

Based on multiple decades of both modeling and observational studies, it seems generally apparent that the secondary circulations that can be generated by coherent land-surface patterns, and thus the underlying spatial scale of land-surface heterogeneity, are important for ABL development (Albertson et al., 2001; Chen & Avissar, 1994; Hadfield et al., 1992; Kang & Ryu, 2016; Letzel & Raasch, 2003; Patton et al., 2005; Shen & Leclerc, 1995; Sühring et al., 2014; Timmermans et al., 2008; Trier et al., 2004; van Heerwaarden et al., 2014). From the results seen in Section 3.1 we can see more specifically the relevance to modern global model dynamics and parameterizations, where heterogeneous land-atmosphere interactions which would be on the SGS in a typical global ESM have a significant impact on the LWP and TKE signals which would be on the grid scale in the same typical ESM. The results in Section 3.2 further elucidate the situation, as well as the associated difficulties, by showing that the most significant driver of SGS land-surface heterogeneity for a global model is SGS atmospheric heterogeneity. This cycle of rainfall patterns which lead to

land-surface heterogeneity which triggers deep convection and restarts the cycle has also been suggested in previous studies (Emori, 1998; Lynn et al., 1998; Taylor et al., 2012; Weaver, 2004a, 2004b).

The LES experiments presented here are an initial investigation into the effects of realistic land-surface and atmospheric heterogeneity which is on the SGS in a typical global model, and are intended to be built upon with the ultimate goal of providing useful numerical data for climate-scale diagnostic and parameterization development. The land-surface fields used to drive the LESs are from a diurnal cycle in a spun-up and fully functional LSM using real datasets for land cover, soil type, surface-routing terrain, and meteorology. The fields from the LSM are also assimilated with the observationally improved VARANAL data set, further ensuring realistic energetics in the land surface. The spatial resolution and domain size are both also significant, with $\Delta_{x,y} = 100$ m over the 100×100 km^2 domain and $\Delta_z = 30$ m in the lower 5 km of the vertical column. In this regard, the simulations conducted here offer a significant and novel increase in realism toward the study of the coupling between land and atmosphere heterogeneity in an ESM. However, there are still many idealizations made in the simulations presented which warrant mentioning and examining further in future studies. The two most notable idealizations used here are: the semi-coupled LSM, where the land surface fields are specified *a priori* and do not receive feedback from the atmosphere as it is simulated, and, the periodic lateral boundary conditions.

The lack of a feedback between the atmosphere and the land surface means that clouds that develop do not impact the local radiation budget of the land surface. Rieck et al. (2014), using a fully coupled LSM, found that the shading effect from clouds reduced the difference between sensible heat fluxes over warm/dry and cool/moist patches by 20%, suggesting that resolved mesoscale circulations would indeed be too strong without atmosphere-to-land coupling. The potential shading feedback may not be as strong in the case considered here, as the case in Rieck et al. (2014) has a minimal background wind speed of 0.5 m s^{-1}, compared to the approximately 15 m s^{-1} background wind used here. Such advection of clouds away from their source significantly complicates the nature of atmosphere-to-land feedback (as noted by Weaver & Avissar, 2001). Also, the chessboard pattern used to generate land-surface heterogeneity in Rieck et al. (2014) means that each warm/dry patch is bordered on all four sides by a cool/moist patch, resulting in a much more uniform cloud cover over the warm patches in their study than seen here. Still, the extension of our study to a fully coupled LSM is a necessary next step which is currently under development by the co-authors and will provide valuable insights into both the model requirements for an LES with highly heterogeneous land-surface fields and the degree of feedback from atmospheric heterogeneity to the land surface from a physical (though numerical) perspective.

The periodic lateral boundary conditions used in the simulations, while standard practice for LES and cloud-resolving studies, is another concession which potentially influences the results seen here. The cloud production in the no wind case in Section 3.3 shows a significant temporal and spatial response to land-surface heterogeneity with a very visible preference for production over drier areas of the land surface. It can thus be assumed that the observed results in the cases with wind are not reliant on the continual recycling of moist air across the domain. However, it is not clear how dependent the results are on the sustained fetches of high sensible heat adjacent to high latent heat that are created by the periodic boundaries. The 100×100 km^2 domain used is large enough to fully encapsulate the moist patch in the September 24, 2017 case, but, while it is plausible to imagine, it cannot be assumed that similar patterns are repeated over the surrounding landscape. In conjunction with the fully coupled simulations mentioned above, nested simulations are also being developed to investigate the influence of the periodic lateral boundary conditions used here.

It should also be mentioned that, while $\Delta_{x,y} = 100$ m is a very high resolution in the cloud-resolving arena, the horizontal resolution does present another potential source for improvement. Multiple idealized studies of the so-called gray zone as it relates to resolving the ABL in an LES have found $\Delta_{x,y} = 100$ m to be a sufficient horizontal resolution while $\Delta_{x,y} = 200$ m begins to show signs of grid-dependent turbulence development (e.g., Beare, 2014; Efstathiou & Beare, 2015; J. S. Simon et al., 2019). By this standard, the resolution used here is within the limits of LES. It is not immediately clear how directly these and other idealized gray zone studies, which typically use uniform and constant surface sensible heat fluxes, translate to more realistic surface fluxes. In the simulations here, there is a small burst of resolved TKE at $t \approx 0800$ LST in most of the cases (e.g., Figure 5b), which is a common characteristic of an artificially delayed onset of resolved turbulence due to the turbulence closure model. Such an artifact does not necessarily indicate that

the resolution is irredeemably coarse, so long as the delay of resolved turbulence is not significant and the overall dynamics are accurately simulated once turbulence is triggered. While the effect of the resolution seen here does not appear to be excessive, the effects of the horizontal resolution cannot fully be appreciated without comparison to even finer, as well as coarser, simulations of the same case. Such a study is currently under development and is anticipated to provide novel insights toward understanding land and atmosphere heterogeneity, as well as the gray zone of LES turbulence closure models in general.

Planned future work generally falls into one or both of two categories: clarifying the impact of different aspects of the LES configuration on cases with heterogeneous land surfaces, and, providing value to ongoing efforts toward diagnosing and modeling SGS heterogeneity in ESM parameterizations. On the clarification side, the aforementioned three studies (semi- vs. fully coupled land surfaces, periodic vs. nested lateral boundary conditions, and an expanded range of horizontal resolutions) are the top priorities in the near future. Related to aiding diagnostic and parameterization efforts, the most immediate future work is focused on running heterogeneous and homogeneous simulations for multiple dozen additional days, with various initial conditions on the surface and in the atmosphere, at the SGP site aided by the available data from the LASSO campaign. In the longer term, we plan to extend simulations to additional locations around the globe where different forms of surface heterogeneity may be studied, for example, lakes, mountainous terrain, urban areas. These future studies are not exclusive efforts but will be conducted in conjunction with each other, that is, model configuration choices will be tested for different days and locations, and knowledge gained regarding model behavior will be applied to the diagnostic and parameterization efforts when useful.

5. Summary and Conclusions

Realistic land-surface fields are used to evaluate the role of land-surface heterogeneity on atmospheric dynamics, particularly at the grid-scale of a modern global model, by using high-resolution output from the HydroBlocks LSM to specify spatially heterogeneous and time-evolving surface conditions for sensible heat flux, latent heat flux, temperature (via emissivity and upward longwave radiation), albedo, and drag coefficient in the WRF model. High-resolution LES cases are then run in a variety of experiments over a domain centered at the SGP site which is sized to mimic a single grid cell in a global model. The primary experiment (Section 3.1) compares two simulations of the diurnal cycle on September 24, 2017: the first using the aforementioned heterogeneous surface fields and the second using time-evolving but spatially homogeneous surface fields, which take their uniform value of each field as the domain-average of the field in the heterogeneous case. It is observed that the heterogeneous case produces clouds more actively than the homogeneous case and in a spatial pattern that is correlated to the surface sensible heat flux fields. It is shown that the heterogeneous simulation develops a circulation pattern between moist and dry areas where moist air originating over areas of high surface latent heat flux are transported laterally within the boundary layer to areas of high surface sensible heat flux, and are then lifted upwards through the boundary layer leading to cloud production.

Experiments are then presented to elucidate the relative impacts of specific sources of land-surface heterogeneity for this case (Section 3.2). It is found that spatial patterns created in the land surface by recent rain events are effectively responsible for the entirety of the differences between the atmospheric response in the heterogeneous and homogeneous cases. Contrarily, spatial patterns introduced in the land surface by rivers and subsurface flow have a negligible impact on domain-wide LWP and TKE production compared to the case with the same total surface sensible and latent heat fluxes using fully homogeneous surface values. Spatial patterns from different soil types also show a negligible impact. Introducing heterogeneity from land cover does introduce a nontrivial increase to both LWP and TKE production compared to the homogeneous case, however the effect from land cover becomes trivial once heterogeneity from the forcing meteorology is introduced.

Modifications of the fully heterogeneous case, where the Bowen ratio at each grid cell is increased and where the background wind profile is changed, are then presented to add clarity to the results seen (Section 3.3). It is seen in the cases where the Bowen ratio is increased that the increase in sensible heat is associated with a decrease in cloud production, confirming that the water vapor transported by the emergent

circulation pattern is critical for the high rates of cloud production seen in the heterogeneous case. We also see that re-orienting the prevailing wind in the atmosphere will correspondingly re-orient the cloud-production pattern to remain focused over the dry areas, and that removing the mean wind entirely allows clouds to form everywhere that is associated with a high surface sensible heat flux.

The last set of additional experiments is a brief analysis of two other summer days at the SGP site, both also with large, but unique, scales of spatial heterogeneity generated by scattered storms at the site on previous days (Section 3.4). Both additional days show a significantly larger domain-wide LWP values in the heterogeneous cases compared to their homogeneous counterparts. While the analysis presented here is largely for a single day, these two additional cases strengthen the conclusion that, in the context of SGS parameterizations for global ESMs, land-atmosphere coupling of SGS heterogeneity has a significant impact on grid-scale cloud and turbulence production.

From the results seen here, the three questions posed in Section 1 can be answered with relatively high confidence for the SGP area. First, the mesoscale circulations between wet and dry patches in idealized land surface which have been reported in many LES studies are indeed still present using highly realistic land surfaces and under highly realistic atmospheric conditions, namely a significant background wind. Second, considering an LES domain sized to mimic a single grid cell in a global ESM, the macroscale (domain-wide) atmospheric response to high-resolution land-surface heterogeneity is a significant change to total cloud production which should be included in the grid-scale signal. Third, the heterogeneity created in the soil moisture by meteorological patterns has a significant influence on ABL processes (namely cloud and TKE production), while the heterogeneities created in the land surface by rivers and surface water, soil type, and land cover have a relatively small, but non-zero, impact on ABL development. It follows that SGS cloud and turbulence parameterizations for weather and climate models should also include information about SGS land-surface heterogeneity and vice versa, though an effective mechanism to do so is yet undeveloped. We hope that this and future work will aid in the development of such mechanisms.

Data Availability Statement

Simulations here use a modification of WRF version 3.8.1 developed and maintained by the LASSO team. The base WRF code, initial sounding files, and large-scale forcing files are available from W. Gustafson et al. (2019). Additional modifications to the WRF code to specify heterogeneous surfaces, data files for surface fields for each simulation, and model control files for each simulation are available at Simon and Chaney (2021).

Acknowledgments
Funded by NOAA grant NA19OAR4310241. PD's contribution is funded by NOAA grant NA19OAR4310242.

References

Albertson, J. D., Kustas, W. P., & Scanlon, T. M. (2001). Large-eddy simulation over heterogeneous terrain with remotely sensed land surface conditions. *Water Resources Research*, *37*(7), 1939–1953. https://doi.org/10.1029/2000wr900339

Avissar, R., & Liu, Y. (1996). Three-dimensional numerical study of shallow convective clouds and precipitation induced by land surface forcing. *Journal of Geophysical Research*, *101*(D3), 7499–7518. https://doi.org/10.1029/95jd03031

Avissar, R., & Schmidt, T. (1998). An evaluation of the scale at which ground-surface heat flux patchiness affects the convective boundary layer using large-eddy simulations. *Journal of the Atmospheric Sciences*, *55*(16), 2666–2689. https://doi.org/10.1175/1520-0469(1998)055<2666:aeotsa>2.0.co;2

Barlage, M., Chen, F., Rasmussen, R., Zhang, Z., & Miguez-Macho, G. (2021). The importance of scale-dependent groundwater processes in land-atmosphere interactions over the central United States. *Geophysical Research Letters*, *48*(5), e2020GL092171. https://doi.org/10.1029/2020gl092171

Beare, R. J. (2014). A length scale defining partially-resolved boundary-layer turbulence simulations. *Boundary-Layer Meteorology*, *151*(1), 39–55. https://doi.org/10.1007/s10546-013-9881-3

Bertoldi, G., Kustas, W. P., & Albertson, J. D. (2013). Evaluating source area contributions from aircraft flux measurements over heterogeneous land using large-eddy simulation. *Boundary-Layer Meteorology*, *147*(2), 261–279. https://doi.org/10.1007/s10546-012-9781-y

Bonan, G. B., Oleson, K. W., Vertenstein, M., Levis, S., Zeng, X., Dai, Y., et al. (2002). The land surface climatology of the Community Land Model coupled to the NCAR Community Climate Model. *Journal of Climate*, *15*(22), 3123–3149. https://doi.org/10.1175/1520-0442(2002)015<3123:tlscot>2.0.co;2

Bosman, P. J., van Heerwaarden, C. C., & Teuling, A. J. (2019). Sensible heating as a potential mechanism for enhanced cloud formation over temperate forest. *Quarterly Journal of the Royal Meteorological Society*, *145*(719), 450–468. https://doi.org/10.1002/qj.3441

Bou-Zeid, E., Meneveau, C., & Parlange, M. B. (2004). Large-eddy simulation of neutral atmospheric boundary layer flow over heterogeneous surfaces: Blending height and effective surface roughness. *Water Resources Research*, *40*(2). https://doi.org/10.1029/2003wr002475

Chaney, N. W., Metcalfe, P., & Wood, E. F. (2016). HydroBlocks: A field-scale resolving land surface model for application over continental extents. *Hydrological Processes*, *30*(20), 3543–3559. https://doi.org/10.1002/hyp.10891

Chaney, N. W., Minasny, B., Herman, J. D., Nauman, T. W., Brungard, C. W., Morgan, C. L., et al. (2019). POLARIS soil properties: 30-m probabilistic maps of soil properties over the contiguous United States. *Water Resources Research*, *55*(4), 2916–2938. https://doi.org/10.1029/2018wr022797

Chaney, N. W., Roundy, J. K., Herrera-Estrada, J. E., & Wood, E. F. (2015). High-resolution modeling of the spatial heterogeneity of soil moisture: Applications in network design. *Water Resources Research*, *51*(1), 619–638. https://doi.org/10.1002/2013wr014964

Chaney, N. W., Torres-Rojas, L., Vergopolan, N., & Fisher, C. K. (2020). Two-way coupling between the sub-grid land surface and river networks in Earth system models. *Geoscientific Model Development Discussions*, 1–31. https://doi.org/10.5194/gmd-2020-291

Chaney, N. W., Van Huijgevoort, M. H., Shevliakova, E., Malyshev, S., Milly, P. C., Gauthier, P. P., & Sulman, B. N. (2018). Harnessing big data to rethink land heterogeneity in Earth system models. *Hydrology and Earth System Sciences*, *22*(6), 3311–3330. https://doi.org/10.5194/hess-22-3311-2018

Chaney, N. W., Wood, E. F., McBratney, A. B., Hempel, J. W., Nauman, T. W., Brungard, C. W., & Odgers, N. P. (2016). POLARIS: A 30-meter probabilistic soil series map of the contiguous United States. *Geoderma*, *274*, 54–67. https://doi.org/10.1016/j.geoderma.2016.03.025

Chen, F., & Avissar, R. (1994). Impact of land-surface moisture variability on local shallow convective cumulus and precipitation in large-scale models. *Journal of Applied Meteorology and Climatology*, *33*(12), 1382–1401. https://doi.org/10.1175/1520-0450(1994)033<1382:iolsmv>2.0.co;2

Cheng, W. Y., & Cotton, W. R. (2004). Sensitivity of a cloud-resolving simulation of the genesis of a mesoscale convective system to horizontal heterogeneities in soil moisture initialization. *Journal of Hydrometeorology*, *5*(5), 934–958. https://doi.org/10.1175/1525-7541(2004)005<0934:soacso>2.0.co;2

Clark, M. P., Fan, Y., Lawrence, D. M., Adam, J. C., Bolster, D., Gochis, D. J., et al. (2015). Improving the representation of hydrologic processes in Earth System Models. *Water Resources Research*, *51*(8), 5929–5956. https://doi.org/10.1002/2015wr017096

Cosgrove, B. A., Lohmann, D., Mitchell, K. E., Houser, P. R., Wood, E. F., Schaake, J. C., et al. (2003). Real-time and retrospective forcing in the North American Land Data Assimilation System (NLDAS) project. *Journal of Geophysical Research*, *108*(D22). https://doi.org/10.1029/2002jd003118

Courault, D., Drobinski, P., Brunet, Y., Lacarrere, P., & Talbot, C. (2007). Impact of surface heterogeneity on a buoyancy-driven convective boundary layer in light winds. *Boundary-Layer Meteorology*, *124*(3), 383–403. https://doi.org/10.1007/s10546-007-9172-y

Dixon, N., Parker, D., Taylor, C., Garcia-Carreras, L., Harris, P., Marsham, J., et al. (2013). The effect of background wind on mesoscale circulations above variable soil moisture in the sahel. *Quarterly Journal of the Royal Meteorological Society*, *139*(673), 1009–1024. https://doi.org/10.1002/qj.2012

Doran, J., Shaw, W., & Hubbe, J. (1995). Boundary layer characteristics over areas of inhomogeneous surface fluxes. *Journal of Applied Meteorology and Climatology*, *34*(2), 559–571. https://doi.org/10.1175/1520-0450-34.2.559

Ducharne, A., Koster, R. D., Suarez, M. J., Stieglitz, M., & Kumar, P. (2000). A catchment-based approach to modeling land surface processes in a general circulation model: 2. parameter estimation and model demonstration. *Journal of Geophysical Research*, *105*(D20), 24823–24838. https://doi.org/10.1029/2000jd900328

Eder, F., De Roo, F., Rotenberg, E., Yakir, D., Schmid, H. P., & Mauder, M. (2015). Secondary circulations at a solitary forest surrounded by semi-arid shrubland and their impact on eddy-covariance measurements. *Agricultural and Forest Meteorology*, *211*, 115–127. https://doi.org/10.1016/j.agrformet.2015.06.001

Efstathiou, G., & Beare, R. J. (2015). Quantifying and improving sub-grid diffusion in the boundary-layer grey zone. *Quarterly Journal of the Royal Meteorological Society*, *141*(693), 3006–3017. https://doi.org/10.1002/qj.2585

Emori, S. (1998). The interaction of cumulus convection with soil moisture distribution: An idealized simulation. *Journal of Geophysical Research*, *103*(D8), 8873–8884. https://doi.org/10.1029/98jd00426

Esau, I., & Lyons, T. (2002). Effect of sharp vegetation boundary on the convective atmospheric boundary layer. *Agricultural and Forest Meteorology*, *114*(1–2), 3–13. https://doi.org/10.1016/s0168-1923(02)00154-5

Findell, K. L., & Eltahir, E. A. (2003). Atmospheric controls on soil moisture-boundary layer interactions: Three-dimensional wind effects. *Journal of Geophysical Research*, *108*(D8). https://doi.org/10.1029/2001jd001515

Garcia-Carreras, L., Parker, D. J., & Marsham, J. H. (2011). What is the mechanism for the modification of convective cloud distributions by land surface–induced flows? *Journal of the Atmospheric Sciences*, *68*(3), 619–634. https://doi.org/10.1175/2010jas3604.1

Garcia-Carreras, L., Parker, D. J., Taylor, C. M., Reeves, C. E., & Murphy, J. G. (2010). Impact of mesoscale vegetation heterogeneities on the dynamical and thermodynamic properties of the planetary boundary layer. *Journal of Geophysical Research*, *115*(D3). https://doi.org/10.1029/2009jd012811

Golaz, J.-C., Larson, V. E., & Cotton, W. R. (2002). A PDF-based model for boundary layer clouds. Part I: Method and model description. *Journal of the Atmospheric Sciences*, *59*(24), 3540–3551. https://doi.org/10.1175/1520-0469(2002)059<3540:apbmfb>2.0.co;2

Gómez-Plaza, A., Martınez-Mena, M., Albaladejo, J., & Castillo, V. (2001). Factors regulating spatial distribution of soil water content in small semiarid catchments. *Journal of Hydrology*, *253*(1–4), 211–226. https://doi.org/10.1016/s0022-1694(01)00483-8

Gustafson, W., Vogelmann, A., Cheng, X., Dumas, K., Endo, S., Johnson, K., et al. (2019). *Description of the LASSO data bundles product*. (DOE/SC-ARM-TR-216). DOE Atmospheric Radiation Measurement (ARM) User Facility. https://doi.org/10.2172/1469590

Gustafson, W. I., Vogelmann, A. M., Li, Z., Cheng, X., Dumas, K. K., Endo, S., et al. (2020). The Large-eddy simulation (LES) Atmospheric Radiation Measurement (ARM) Symbiotic Simulation and Observation (LASSO) activity for continental shallow convection. *Bulletin of the American Meteorological Society*, *101*(4), E462–E479. https://doi.org/10.1175/bams-d-19-0065.1

Gutowski, W. J., Ullrich, P. A., Hall, A., Leung, L. R., O'Brien, T. A., Patricola, C. M., et al. (2020). The ongoing need for high-resolution regional climate models: Process understanding and stakeholder information. *Bulletin of the American Meteorological Society*, *101*(5), E664–E683. https://doi.org/10.1175/bams-d-19-0113.1

Hadfield, M., Cotton, W., & Pielke, R. (1991). Large-eddy simulations of thermally forced circulations in the convective boundary layer. Part I: A small-scale circulation with zero wind. *Boundary-Layer Meteorology*, *57*(1), 79–114. https://doi.org/10.1007/bf00119714

Hadfield, M., Cotton, W., & Pielke, R. (1992). Large-eddy simulations of thermally forced circulations in the convective boundary layer. Part II: The effect of changes in wavelength and wind speed. *Boundary-Layer Meteorology*, *58*(4), 307–327. https://doi.org/10.1007/bf00120235

Han, C., Brdar, S., & Kollet, S. (2019). Response of convective boundary layer and shallow cumulus to soil moisture heterogeneity: A large-eddy simulation study. *Journal of Advances in Modeling Earth Systems*, *11*(12), 4305–4322. https://doi.org/10.1029/2019ms001772

Han, C., Brdar, S., Raasch, S., & Kollet, S. (2019). Large-eddy simulation of catchment-scale circulation. *Quarterly Journal of the Royal Meteorological Society*, *145*(720), 1218–1233. https://doi.org/10.1002/qj.3491

Hohenegger, C., Brockhaus, P., Bretherton, C. S., & Schär, C. (2009). The soil moisture–precipitation feedback in simulations with explicit and parameterized convection. *Journal of Climate*, *22*(19), 5003–5020. https://doi.org/10.1175/2009jcli2604.1

Homer, C. H., Fry, J. A., & Barnes, C. A. (2012). The national land cover database. *US Geological Survey Fact Sheet*, *3020*(4), 1–4. https://doi.org/10.3133/fs20123020

Huang, H.-Y., & Margulis, S. A. (2013). Impact of soil moisture heterogeneity length scale and gradients on daytime coupled land-cloudy boundary layer interactions. *Hydrological Processes*, *27*(14), 1988–2003. https://doi.org/10.1002/hyp.9351

Jacobs, J., Mohanty, B., Hsu, E., & Miller, D. (2004). Field scale variability and similarity of soil moisture. *Remote Sensing of Environment*, *92*, 436–446. https://doi.org/10.1016/j.rse.2004.02.017

Kang, S.-L. (2016). Regional Bowen ratio controls on afternoon moist convection: A large eddy simulation study. *Journal of Geophysical Research: Atmospheres*, *121*(23), 14056–14083. https://doi.org/10.1002/2016JD025567

Kang, S.-L. (2020). Effects of mesoscale surface heterogeneity on the afternoon and early evening transition of the atmospheric boundary layer. *Boundary-Layer Meteorology*, *174*(3), 371–391. https://doi.org/10.1007/s10546-019-00493-w

Kang, S.-L., & Bryan, G. H. (2011). A large-eddy simulation study of moist convection initiation over heterogeneous surface fluxes. *Monthly Weather Review*, *139*(9), 2901–2917. https://doi.org/10.1175/mwr-d-10-05037.1

Kang, S.-L., & Lenschow, D. H. (2014). Temporal evolution of low-level winds induced by two-dimensional mesoscale surface heat-flux heterogeneity. *Boundary-Layer Meteorology*, *151*(3), 501–529. https://doi.org/10.1007/s10546-014-9912-8

Kang, S.-L., & Ryu, J.-H. (2016). Response of moist convection to multi-scale surface flux heterogeneity. *Quarterly Journal of the Royal Meteorological Society*, *142*(698), 2180–2193. https://doi.org/10.1002/qj.2811

Khanal, S., Wang, Z., & French, J. R. (2020). Improving middle and high latitude cloud liquid water path measurements from MODIS. *Atmospheric Research*, *243*, 105033. https://doi.org/10.1016/j.atmosres.2020.105033

Kim, H.-J., Noh, Y., & Raasch, S. (2002). Interaction between wind and temperature fields under the heterogeneous heat flux in the planetary boundary layer. In *15th conference on boundary layer and turbulence*.

Koster, R. D., Suarez, M. J., Higgins, R. W., & Van den Dool, H. M. (2003). Observational evidence that soil moisture variations affect precipitation. *Geophysical Research Letters*, *30*(5). https://doi.org/10.1029/2002gl016571

Kustas, W. P., & Albertson, J. D. (2003). Effects of surface temperature contrast on land-atmosphere exchange: A case study from monsoon 90. *Water Resources Research*, *39*(6). https://doi.org/10.1029/2001wr001226

Lawrence, D. M., Fisher, R. A., Koven, C. D., Oleson, K. W., Swenson, S. C., Bonan, G., et al. (2019). The Community Land Model version 5: Description of new features, benchmarking, and impact of forcing uncertainty. *Journal of Advances in Modeling Earth Systems*, *11*(12), 4245–4287. https://doi.org/10.1029/2018ms001583

Lee, J. M., Zhang, Y., & Klein, S. A. (2019). The effect of land surface heterogeneity and background wind on shallow cumulus clouds and the transition to deeper convection. *Journal of the Atmospheric Sciences*, *76*(2), 401–419. https://doi.org/10.1175/jas-d-18-0196.1

Letzel, M. O., & Raasch, S. (2003). Large eddy simulation of thermally induced oscillations in the convective boundary layer. *Journal of the Atmospheric Sciences*, *60*(18), 2328–2341. https://doi.org/10.1175/1520-0469(2003)060<2328:lesoti>2.0.co;2

Lin, Y., & Mitchell, K. E. (2005). The NCEP stage II/IV hourly precipitation analyses: Development and applications In *Proceedings of the 19th conference hydrology* (Vol. 10). San Diego, CA: American Meteorological Society.

Lynn, B. H., Tao, W.-K., & Wetzel, P. J. (1998). A study of landscape-generated deep moist convection. *Monthly Weather Review*, *126*(4), 928–942. https://doi.org/10.1175/1520-0493(1998)126<0928:asolgd>2.0.co;2

Lyons, T. (2002). Clouds prefer native vegetation. *Meteorology and Atmospheric Physics*, *80*(1), 131–140. https://doi.org/10.1007/s007030200020

Lyons, T., Schwerdtfeger, P., Hacker, J., Foster, I., Smith, R., & Xinmei, H. (1993). Land-atmosphere interaction in a semiarid region: The bunny fence experiment. *Bulletin of the American Meteorological Society*, *74*(7), 1327–1334. https://doi.org/10.1175/1520-0477(1993)074<1327:liiasr>2.0.co;2

Maronga, B., & Raasch, S. (2013). Large-eddy simulations of surface heterogeneity effects on the convective boundary layer during the LITFASS-2003 experiment. *Boundary-Layer Meteorology*, *146*(1), 17–44. https://doi.org/10.1007/s10546-012-9748-z

Marsham, J. H., Parker, D. J., Grams, C. M., Johnson, B. T., Grey, W. M., & Ross, A. N. (2008). Observations of mesoscale and boundary-layer scale circulations affecting dust transport and uplift over the Sahara. *Atmospheric Chemistry and Physics*, *8*(23), 6979–6993. https://doi.org/10.5194/acp-8-6979-2008

Mendes, C. B., & Prevedello, J. A. (2020). Does habitat fragmentation affect landscape-level temperatures? A global analysis. *Landscape Ecology*, *35*(8), 1743–1756. https://doi.org/10.1007/s10980-020-01041-5

Milly, P. C., Malyshev, S. L., Shevliakova, E., Dunne, K. A., Findell, K. L., Gleeson, T., et al. (2014). An enhanced model of land water and energy for global hydrologic and earth-system studies. *Journal of Hydrometeorology*, *15*(5), 1739–1761. https://doi.org/10.1175/jhm-d-13-0162.1

Mitchell, K. E., Lohmann, D., Houser, P. R., Wood, E. F., Schaake, J. C., Robock, A., et al. (2004). The multi-institution North American Land Data Assimilation System (NLDAS): Utilizing multiple GCIP products and partners in a continental distributed hydrological modeling system. *Journal of Geophysical Research: Atmospheres*, *109*(D7). https://doi.org/10.1029/2003jd003823

Niu, G.-Y., Yang, Z.-L., Mitchell, K. E., Chen, F., Ek, M. B., Barlage, M., et al. (2011). The community Noah land surface model with multiparameterization options (Noah-MP): 1. model description and evaluation with local-scale measurements. *Journal of Geophysical Research: Atmospheres*, *116*(D12). https://doi.org/10.1029/2010jd015139

Ntelekos, A. A., Smith, J. A., Baeck, M. L., Krajewski, W. F., Miller, A. J., & Goska, R. (2008). Extreme hydrometeorological events and the urban environment: Dissecting the 7 July 2004 thunderstorm over the Baltimore MD Metropolitan Region. *Water Resources Research*, *44*(8). https://doi.org/10.1029/2007wr006346

Patton, E. G., Sullivan, P. P., & Moeng, C.-H. (2005). The influence of idealized heterogeneity on wet and dry planetary boundary layers coupled to the land surface. *Journal of the Atmospheric Sciences*, *62*(7), 2078–2097. https://doi.org/10.1175/jas3465.1

Phillips, T. J., & Klein, S. A. (2014). Land-atmosphere coupling manifested in warm-season observations on the US southern great plains. *Journal of Geophysical Research: Atmospheres*, *119*(2), 509–528. https://doi.org/10.1002/2013jd020492

Pielke Sr, R. A. (2001). Influence of the spatial distribution of vegetation and soils on the prediction of cumulus convective rainfall. *Reviews of Geophysics*, *39*(2), 151–177. https://doi.org/10.1029/1999rg000072

Prabha, T. V., Karipot, A., & Binford, M. W. (2007). Characteristics of secondary circulations over an inhomogeneous surface simulated with large-eddy simulation. *Boundary-Layer Meteorology*, *123*(2), 239–261. https://doi.org/10.1007/s10546-006-9137-6

Raasch, S., & Harbusch, G. (2001). An analysis of secondary circulations and their effects caused by small-scale surface inhomogeneities using large-eddy simulation. *Boundary-Layer Meteorology*, *101*(1), 31–59. https://doi.org/10.1023/a:1019297504109

Rieck, M., Hohenegger, C., & van Heerwaarden, C. C. (2014). The influence of land surface heterogeneities on cloud size development. *Monthly Weather Review*, *142*(10), 3830–3846. https://doi.org/10.1175/mwr-d-13-00354.1

Rochetin, N., Couvreux, F., & Guichard, F. (2017). Morphology of breeze circulations induced by surface flux heterogeneities and their impact on convection initiation. *Quarterly Journal of the Royal Meteorological Society*, *143*(702), 463–478. https://doi.org/10.1002/qj.2935

Senatore, A., Mendicino, G., Gochis, D. J., Yu, W., Yates, D. N., & Kunstmann, H. (2015). Fully coupled atmosphere-hydrology simulations for the central Mediterranean: Impact of enhanced hydrological parameterization for short and long time scales. *Journal of Advances in Modeling Earth Systems*, *7*(4), 1693–1715. https://doi.org/10.1002/2015ms000510

Sengupta, M., Clothiaux, E. E., Ackerman, T. P., Kato, S., & Min, Q. (2003). Importance of accurate liquid water path for estimation of solar radiation in warm boundary layer clouds: An observational study. *Journal of Climate*, *16*(18), 2997–3009. https://doi.org/10.1175/1520-0442(2003)016<2997:ioalwp>2.0.co;2

Shao, Y., Liu, S., Schween, J. H., & Crewell, S. (2013). Large-eddy atmosphere-land-surface modelling over heterogeneous surfaces: Model development and comparison with measurements. *Boundary-Layer Meteorology*, *148*(2), 333–356. https://doi.org/10.1007/s10546-013-9823-0

Shen, S., & Leclerc, M. Y. (1995). How large must surface in homogeneities be before they influence the convective boundary layer structure? A case study. *Quarterly Journal of the Royal Meteorological Society*, *121*(526), 1209–1228. https://doi.org/10.1002/qj.49712152603

Shrestha, P., Sulis, M., Masbou, M., Kollet, S., & Simmer, C. (2014). A scale-consistent terrestrial systems modeling platform based on COSMO, CLM, and ParFlow. *Monthly Weather Review*, *142*(9), 3466–3483. https://doi.org/10.1175/mwr-d-14-00029.1

Simon, J., & Chaney, N. (2021). *Data for: Semi-coupling of a field-scale resolving land-surface model and WRF-LES to investigate the influence of land-surface heterogeneity on cloud development*. Zenodo. https://doi.org/10.5281/zenodo.4741327

Simon, J. S., Zhou, B., Mirocha, J. D., & Chow, F. K. (2019). Explicit filtering and reconstruction to reduce grid dependence in convective boundary layer simulations using WRF-LES. *Monthly Weather Review*, *147*(5), 1805–1821. https://doi.org/10.1175/MWR-D-18-0205.1

Skamarock, W., Klemp, J., Dudhia, J., Gill, D., Barker, D., Duda, M., & Powers, J. (2008). *A description of the advanced research WRF version 3.* (NCAR/TN-475+STR). NCAR Technical Note.

Sühring, M., Maronga, B., Herbort, F., & Raasch, S. (2014). On the effect of surface heat-flux heterogeneities on the mixed-layer-top entrainment. *Boundary-Layer Meteorology*, *151*(3), 531–556. https://doi.org/10.1007/s10546-014-9913-7

Sušelj, K., Teixeira, J., & Chung, D. (2013). A unified model for moist convective boundary layers based on a stochastic eddy-diffusivity/mass-flux parameterization. *Journal of the Atmospheric Sciences*, *70*(7), 1929–1953.

Talbot, C., Bou-Zeid, E., & Smith, J. (2012). Nested mesoscale large-eddy simulations with WRF: Performance in real test cases. *Journal of Hydrometeorology*, *13*(5), 1421–1441. https://doi.org/10.1175/jhm-d-11-048.1

Taylor, C. M., de Jeu, R. A., Guichard, F., Harris, P. P., & Dorigo, W. A. (2012). Afternoon rain more likely over drier soils. *Nature*, *489*(7416), 423–426. https://doi.org/10.1038/nature11377

Taylor, C. M., Gounou, A., Guichard, F., Harris, P. P., Ellis, R. J., Couvreux, F., & De Kauwe, M. (2011). Frequency of Sahelian storm initiation enhanced over mesoscale soil-moisture patterns. *Nature Geoscience*, *4*(7), 430–433. https://doi.org/10.1038/ngeo1173

Timmermans, W., Bertoldi, G., Albertson, J., Olioso, A., Su, Z., & Gieske, A. (2008). Accounting for atmospheric boundary layer variability on flux estimation from rs observations. *International Journal of Remote Sensing*, *29*(17–18), 5275–5290. https://doi.org/10.1080/01431160802036383

Trier, S. B., Chen, F., & Manning, K. W. (2004). A study of convection initiation in a mesoscale model using high-resolution land surface initial conditions. *Monthly Weather Review*, *132*(12), 2954–2976. https://doi.org/10.1175/mwr2839.1

van Heerwaarden, C. C., & de Arellano, J. V. G. (2008). Relative humidity as an indicator for cloud formation over heterogeneous land surfaces. *Journal of the Atmospheric Sciences*, *65*(10), 3263–3277. https://doi.org/10.1175/2008jas2591.1

van Heerwaarden, C. C., Mellado, J. P., & De Lozar, A. (2014). Scaling laws for the heterogeneously heated free convective boundary layer. *Journal of the Atmospheric Sciences*, *71*(11), 3975–4000. https://doi.org/10.1175/jas-d-13-0383.1

Vergopolan, N., Chaney, N. W., Beck, H. E., Pan, M., Sheffield, J., Chan, S., & Wood, E. F. (2020). Combining hyper-resolution land surface modeling with SMAP brightness temperatures to obtain 30-m soil moisture estimates. *Remote Sensing of Environment*, *242*, 111740. https://doi.org/10.1016/j.rse.2020.111740

Weaver, C. P. (2004a). Coupling between large-scale atmospheric processes and mesoscale land–atmosphere interactions in the US southern Great Plains during summer. Part I: Case studies. *Journal of Hydrometeorology*, *5*(6), 1223–1246. https://doi.org/10.1175/jhm-396.1

Weaver, C. P. (2004b). Coupling between large-scale atmospheric processes and mesoscale land–atmosphere interactions in the US southern Great Plains during summer. Part II: Mean impacts of the mesoscale. *Journal of Hydrometeorology*, *5*(6), 1247–1258. https://doi.org/10.1175/jhm-397.1

Weaver, C. P., & Avissar, R. (2001). Atmospheric disturbances caused by human modification of the landscape. *Bulletin of the American Meteorological Society*, *82*(2), 269–281. https://doi.org/10.1175/1520-0477(2001)082<0269:adcbhm>2.3.co;2

Western, A. W., Grayson, R. B., Blöschl, G., Willgoose, G. R., & McMahon, T. A. (1999). Observed spatial organization of soil moisture and its relation to terrain indices. *Water Resources Research*, *35*(3), 797–810. https://doi.org/10.1029/1998wr900065

Zhang, N., Williams, Q. L., & Liu, H. (2010). Effects of land-surface heterogeneity on numerical simulations of mesoscale atmospheric boundary layer processes. *Theoretical and Applied Climatology*, *102*(3), 307–317. https://doi.org/10.1007/s00704-010-0268-9